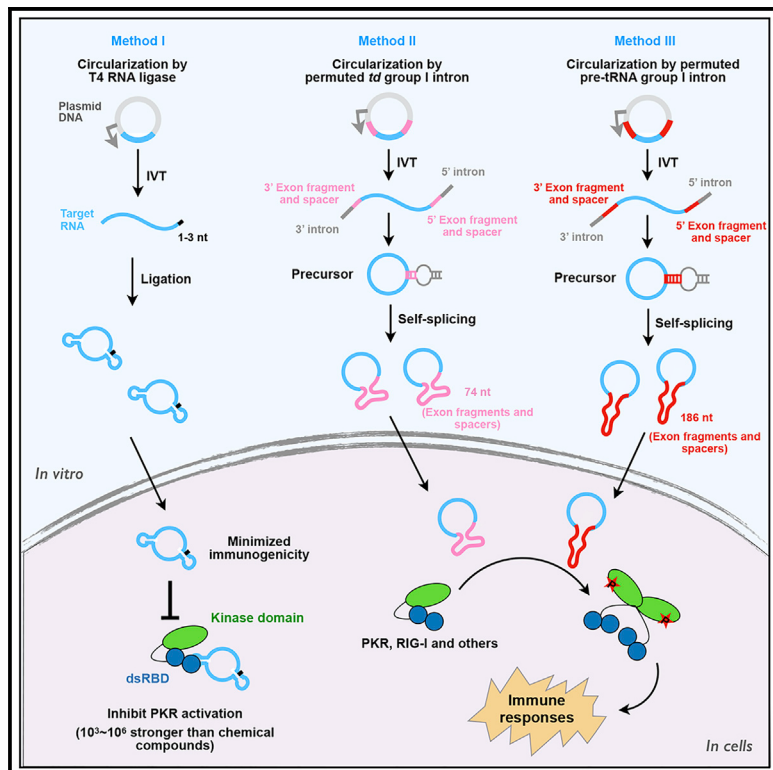


RNA circles with minimized immunogenicity as potent PKR inhibitors

Graphical abstract



Authors

Chu-Xiao Liu, Si-Kun Guo, Fang Nan, Yi-Feng Xu, Li Yang, Ling-Ling Chen

Correspondence

linglingchen@sibcb.ac.cn

In brief

Liu et al. found that extraneous fragments in RNA circles introduced by group I introns provoke immune responses, whereas those produced by RNA ligase exhibit minimized immunogenicity and form short dsRNA regions to efficiently suppress PKR activation.

Highlights

- Synthesized RNA circles by T4 RNA ligase exhibit little immunogenicity
- Extra fragments in RNA circles produced by group I introns provoke immune responses
- RNA circles without extraneous sequences form short dsRNA regions as PKR inhibitors

Article

RNA circles with minimized immunogenicity as potent PKR inhibitors

Chu-Xiao Liu,^{1,5} Si-Kun Guo,^{1,5} Fang Nan,² Yi-Feng Xu,¹ Li Yang,^{2,3} and Ling-Ling Chen^{1,3,4,6,*}

¹State Key Laboratory of Molecular Biology, Shanghai Key Laboratory of Molecular Andrology, CAS Center for Excellence in Molecular Cell Science, Shanghai Institute of Biochemistry and Cell Biology, University of Chinese Academy of Sciences, Chinese Academy of Sciences, 320 Yueyang Road, Shanghai 200031, China

²CAS Key Laboratory of Computational Biology, Shanghai Institute of Nutrition and Health, Shanghai Institutes for Biological Sciences, University of Chinese Academy of Sciences, Chinese Academy of Sciences, 320 Yueyang Road, Shanghai 200031, China

³School of Life Science and Technology, ShanghaiTech University, 100 Haik Road, Shanghai 201210, China

⁴School of Life Science, Hangzhou Institute for Advanced Study, University of Chinese Academy of Sciences, Hangzhou, China

⁵These authors contributed equally

⁶Lead contact

*Correspondence: linglingchen@sibcb.ac.cn

<https://doi.org/10.1016/j.molcel.2021.11.019>

SUMMARY

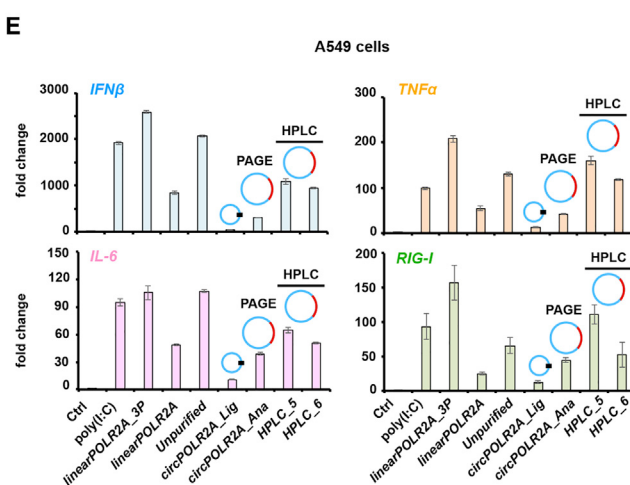
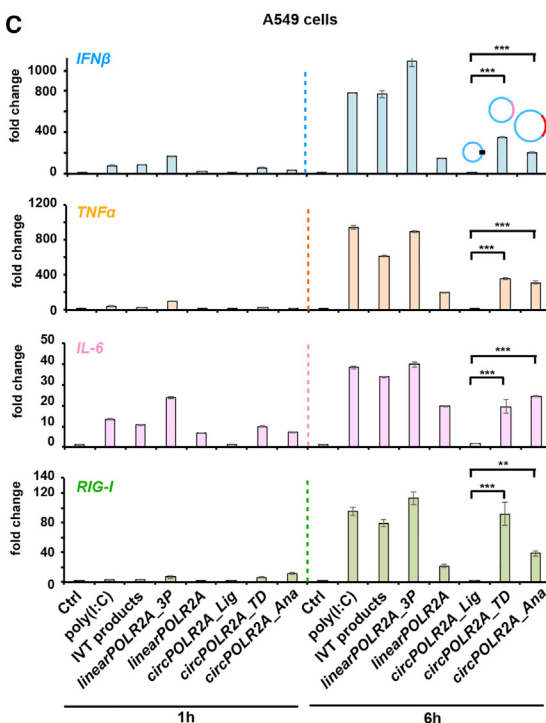
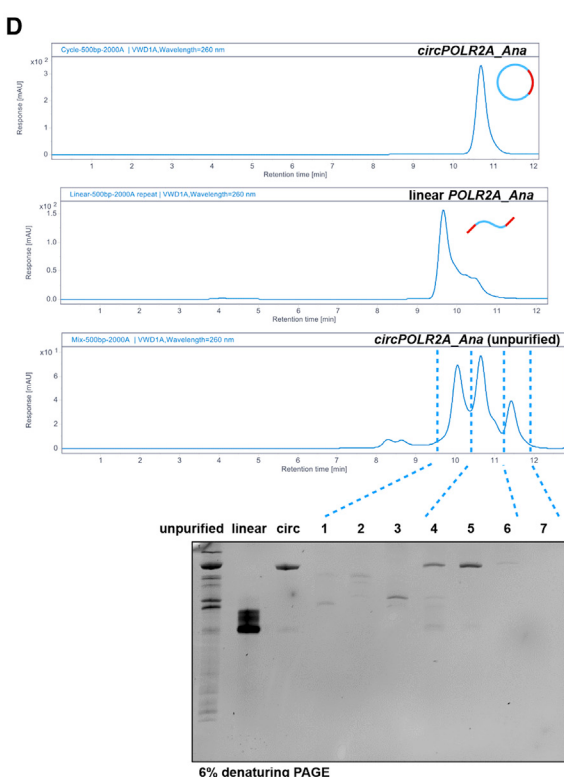
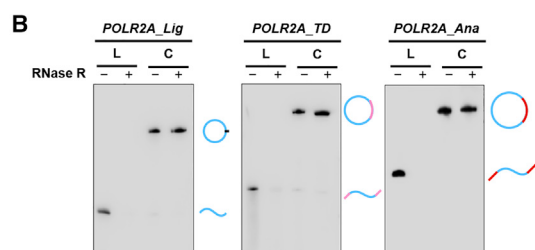
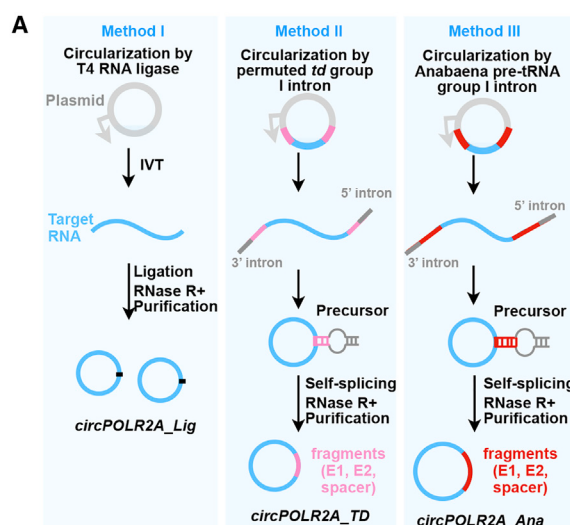
Exon back-splicing-generated circular RNAs, as a group, can suppress double-stranded RNA (dsRNA)-activated protein kinase R (PKR) in cells. We have sought to synthesize immunogenicity-free, short dsRNA-containing RNA circles as PKR inhibitors. Here, we report that RNA circles synthesized by permuted self-splicing thymidylate synthase (*td*) introns from T4 bacteriophage or by Anabaena pre-tRNA group I intron could induce an immune response. Autocatalytic splicing introduces ~74 nt *td* or ~186 nt Anabaena extraneous fragments that can distort the folding status of original circular RNAs or form structures themselves to provoke innate immune responses. In contrast, synthesized RNA circles produced by T4 RNA ligase without extraneous fragments exhibit minimized immunogenicity. Importantly, directly ligated circular RNAs that form short dsRNA regions efficiently suppress PKR activation 10³- to 10⁶-fold higher than reported chemical compounds C16 and 2-AP, highlighting the future use of circular RNAs as potent inhibitors for diseases related to PKR overreaction.

INTRODUCTION

Back-splicing of an exon or exons leads to the production of covalently closed circular RNAs (circRNAs) that are widely expressed in eukaryotes in a tissue- and cell-specific manner. Recent studies have revealed that the production of circRNA is regulated by *cis*-complementary elements in flanking introns and dsRNA binding *trans*-factors related to innate immune responses (Li, 2017; Liu et al., 2019). In addition to reported roles of circRNAs in neuronal functions and cancer progression (for reviews, see Chen, 2020; Xiao et al., 2020), many circRNAs in cells tend to form 16–26 bp imperfect dsRNA regions that act as a group to suppress the activation of the innate immune dsRNA receptor, PKR (Liu et al., 2019). Upon certain virus infections, circRNAs are rapidly degraded, allowing PKR to be involved in cellular innate immune responses (Liu et al., 2019). Global circRNA reduction and enhanced PKR phosphorylation are found in peripheral blood mononuclear cells (PBMCs) derived from patients with the autoimmune disease systemic lupus erythematosus (SLE). Introducing short dsRNA-containing circRNAs by expression vectors in SLE patient-derived PBMCs or T cells alleviated the aberrant PKR activation cascade (Liu et al., 2019). Similar global circRNA reduction

was observed in lesional relative to nonlesional skin with chronic inflammatory skin diseases (Moldovan et al., 2019, 2021). These studies suggest that supplements of immunogenicity-free circularized RNAs may represent a therapeutic potential in PKR-related autoimmune diseases.

Different from endogenous circRNAs that dampen innate immune responses related to PKR (Liu et al., 2019), *in vitro* circularized RNAs using two different group I catalytic introns appear to have distinct immunogenicity (Chen et al., 2017; Wesselhoeft et al., 2019). On the one hand, the addition of *in vitro* synthesized RNA circles generated by the group I intron of the phage T4 *td* gene to cultured mammalian cells induced remarkable immune responses via recognition by the pattern recognition receptor retinoic-acid-inducible gene I (RIG-I) (Chen et al., 2017, 2019), whereas m⁶A modification on circular RNAs in cells could bypass these responses (Chen et al., 2019). Although RIG-I is well known to sense 5'-triphosphate for immune monitoring (Hornung et al., 2006; Reikine et al., 2014), unmodified circular RNAs were found to interact with RIG-I in the presence of K63-Ub_n to induce the immune cascade, which was less robust than dsRNA with 5'-triphosphate ends (Chen et al., 2019). On the other hand, another report has suggested that *in vitro* synthesized unmodified circular RNAs by a



(legend on next page)

Molecular Cell

Article



permuted Anabaena (Ana) pre-tRNA group I intron did not induce responses of cellular RNA sensors including RIG-I and Toll-like receptors (TLRs) in cells (Wesselhoeft et al., 2019). Because of the well-known immune responses induced by *in vitro* synthesized linear RNAs (Safran et al., 2019; Schlee and Hartmann, 2016; Warren et al., 2010), the latter study thus argued that the possible contamination of linear RNA precursors in *in vitro* circularized RNAs might be the cause of the observed immune responses in the former observation. However, because of the nonnegligible existence of remnant fragments (Chen et al., 2017, 2019; Wesselhoeft et al., 2018, 2019) of the construct sequences in both cases of *in vitro* circularized RNAs, factors other than linear RNA contamination (Gholamalipour et al., 2019; Safran et al., 2019) should be further evaluated to reconcile discordant results in the immunogenicity of *in vitro* circularized RNAs (Chen et al., 2017, 2019; Wesselhoeft et al., 2018, 2019). This is critical for their application, such as in modulating immune responses and as vehicles for mRNA translation.

Here, we compare the cellular immune response of *in vitro* circularized and unmodified RNAs via the direct ligation method with T4 RNA ligase, as well as via self-splicing with two group I autocatalytic introns, as mentioned earlier (Figure 1A). Our results show that circularized RNAs produced by self-splicing with either the T4 bacteriophage *td* group I intron or the permuted Anabaena pre-tRNA group I intron can stimulate cellular innate immune responses. Biochemical and structural analyses suggest that self-catalytic splicing can introduce extra fragments (E1, E2, and spacer) from *td* or pre-tRNA genes that likely provoke immune responses. Importantly, direct ligation via T4 RNA ligase without extraneous fragments produces short dsRNA-containing RNA circles with minimized immunogenicity that exhibit a significantly higher inhibitory effect than commonly used chemical compounds on PKR activation both *in vitro* and in cells.

RESULTS

RNA circularization by different strategies *in vitro*

We attempted to synthesize immunogenicity-free circular RNAs as potential therapeutics for PKR-related autoimmune diseases.

Three reported *in vitro* RNA circularization strategies were applied to generate exogenous circular RNAs (Figure 1A). Method I was designed to generate circular RNAs by direct ligation via T4 RNA ligase of *in vitro* transcribed RNAs (Liu et al., 2019; Schindewolf et al., 1996). Method II was performed employing permuted *td* intron autocatalytic splicing from the T4 bacteriophage (Chen et al., 2017; Wesselhoeft et al., 2018). Method III was carried out via a permuted Anabaena pre-tRNA group I autocatalytic intron (Wesselhoeft et al., 2018, 2019). Using *circPOLR2A* as an example, we named these circularized RNAs as *circPOLR2A_Lig* (336 nt) by method I, *circPOLR2A_TD* (410 nt) by method II, and *circPOLR2A_Ana* (522 nt) by method III.

All *in vitro* circularized RNAs were first purified by gel excision of the exact circular RNA bands on denaturing polyacrylamide gel electrophoresis (PAGE) followed by RNase R digestion to remove potential linear RNA contamination (Figure 1B). Here, we treated the samples with RNase R for 45 min (see STAR Methods), and different batches of RNase R were pre-evaluated for the use of optimal concentrations (Zhang et al., 2016b). *In vitro* circularized junction sites of these *circPOLR2A* by all three methods were confirmed with Sanger sequencing (Figure S1A). *circPOLR2A_Lig* introduced 1 to 3 extra guanine (G) nucleotides at the junction site during *in vitro* transcription, and *circPOLR2A_TD* and *circPOLR2A_Ana* introduced ~74 and ~186 extra nucleotides into RNA circles, respectively, after autocatalytic circularization at the junction sites.

Next, we evaluated the circularization efficiency of these methods for RNAs of different lengths. We examined three circular RNAs (*circPOLR2A*, 336 nt; *circmCherry*, 1,452 nt; and *circRTN4*, 2,457 nt) using the same procedures. In our hands, method I could efficiently produce *circPOLR2A_Lig* but worked less efficiently for *circmCherry_Lig* and barely for *circRTN4_Lig* (Figure S1B), suggesting limited circularization capacity by direct ligation with T4 RNA ligase, probably because it is harder to bring the termini together for the ligase when the RNA is longer. In contrast, methods II and III produced *circPOLR2A* and other relatively short RNA circles (data not shown) with efficiency comparable to that of method I, but they could also generate long circular RNAs (>1,000 nt) more efficiently than method I did (Figure S1C).

Figure 1. Circularized RNAs produced by different strategies induce distinct immune responses

- (A) Schematic of *in vitro* circularization and purification of circular RNAs, using *circPOLR2A* as an example. Left, method I, a target RNA is produced by *in vitro* transcription (IVT) from a DNA template and circularized by T4 RNA ligase. Middle, method II, a target RNA is produced by IVT and circularized by phage T4 *td* group I intron autocatalytic splicing (Chen et al., 2017; Wesselhoeft et al., 2018). Right, method III, a target RNA is produced by IVT and circularized by permuted Ana pre-tRNA group I intron autocatalytic splicing (Wesselhoeft et al., 2019).
- (B) Circular RNAs produced using methods I–III were examined by northern blotting. Circular RNAs were purified via denaturing PAGE following band excision and confirmed by RNase R digestion.
- (C) Short circular RNAs, *circPOLR2A*, produced via group I intron splicing (methods II and III) stimulate immune responses, whereas those produced from direct ligation (method I) yielded minimized immunogenicity.
- (D) HPLC resolved *circPOLR2A_Ana* and its linear products into different peaks. The *POLR2A* circle produced by method III was purified by HPLC using the same experimental condition as previously described (Chen et al., 2019; Wesselhoeft et al., 2019). Collection of each fraction (fractions 1–7) reflected HPLC peaks 1–3, and the results of denaturing PAGE showed that peak 2 (fractions 5 and 6) from HPLC has *circPOLR2A_Ana* without linear products.
- (E) HPLC-purified *circPOLR2A_Ana* retained an immune response to a comparable level of *circPOLR2A_Ana* purified by RNase R and gel extraction (see also Figure 1B).
- In (C) and (E), the same amounts (200 ng for each sample) of unmodified *circPOLR2A_Lig*, *circPOLR2A_TD*, and *circPOLR2A_Ana*, as well as linear RNAs with different treatments, were individually transfected into A549 cells. Relative expression of innate immune genes in A549 cells after 6 h of transfection are measured by qRT-PCR, with relative fold change normalized to expression of control (Ctrl; mock) transfection. Error bars represent SD. ***p* < 0.01, ****p* < 0.001, Student's *t* test.

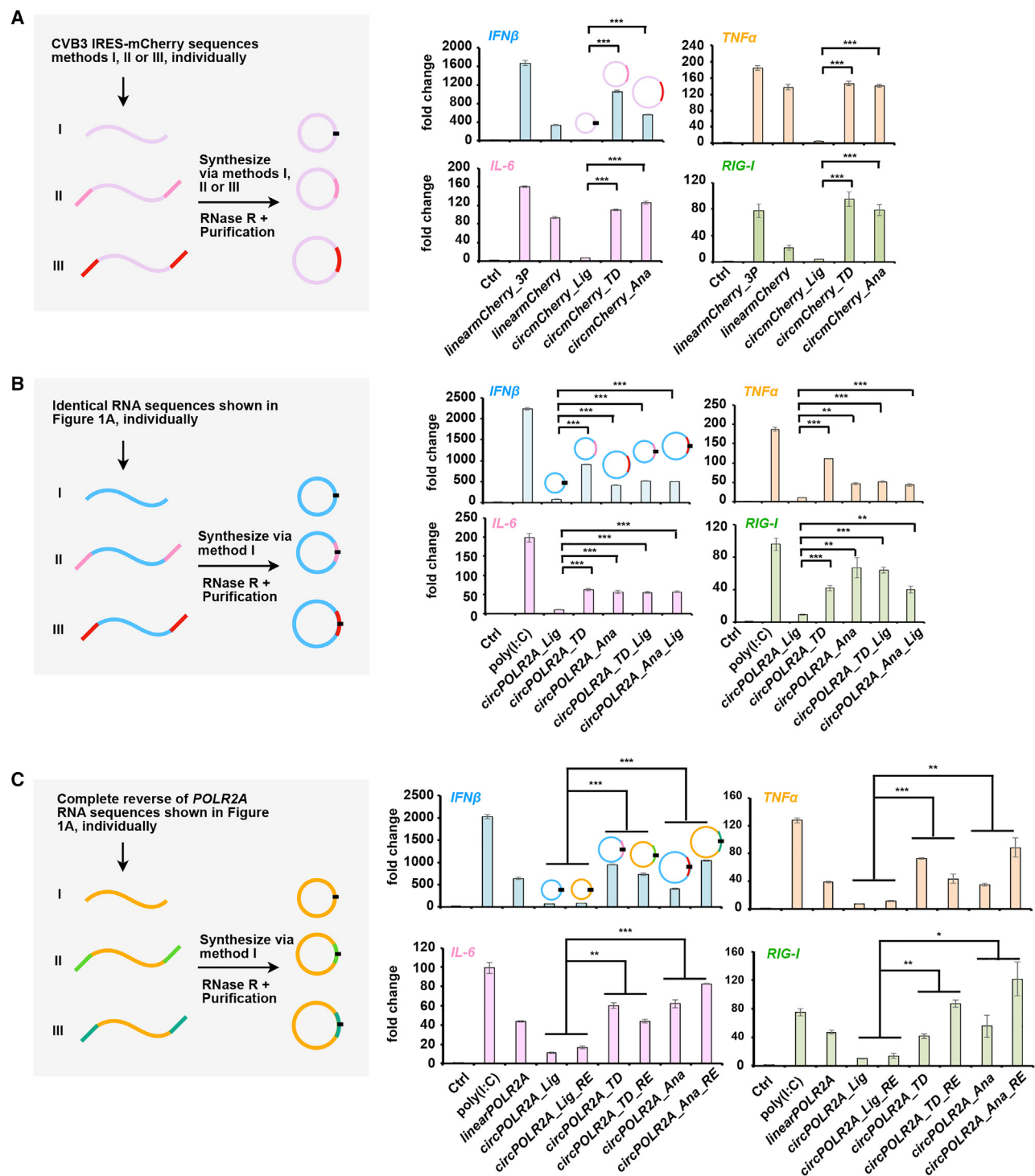


Figure 2. Autocatalytic splicing introduces ~74 nt td and ~186 nt pre-tRNA extraneous fragments in circular RNAs, which likely provoke immune responses

(A) Long circular RNAs, *circmCherry*, produced via group I intron autocatalytic splicing (methods II and III) stimulate immune responses, whereas those produced from direct ligation (method I) do not. Left, schematic of synthesis of *circmCherry* by three strategies. Right, same amounts (200 ng for each sample) of unmodified *circmCherry_Lig*, *circmCherry_TD*, and *circmCherry_Ana*, as well as 5'-triphosphorylated linear *mCherry_3P* and unmodified linear *mCherry*, were individually transfected into A549 cells for 6 h.

(legend continued on next page)

Similar to observations with endogenous circRNAs (Zhang et al., 2014, 2016b), *in vitro* circularized RNAs migrate more slowly than linear precursor RNAs with same sequences on urea denaturing gels but run normally on native agarose gels in accordance to their molecular sizes. Thus, it is important to appreciate the different migration phenomena of circular RNAs on urea denaturing gels or native agarose gels (Figure S2), especially for products after *in vitro* synthesis, when distinctions between circularized RNAs and their precursor linear RNAs can be overlooked.

Previous studies have reported that circular RNAs are more stable than linear RNAs in cells due to their resistance to exonucleolytic degradation (Enuka et al., 2016; Zhang et al., 2016a). Consistently, synthesized circular RNAs were more stable than linear cognate RNAs in examined cells (Figure S3A). Circular RNAs synthesized by different methods likely displayed a cell-type-specific manner of stability, but in general, *circPOLR2A_Lig* was more stable than *circPOLR2A_TD* and *circPOLR2A_Ana* (Figure S3A). Moreover, *in vitro* synthesized circular RNAs, once introduced into cells, were also subjected to the rapid turnover under poly(I:C) stimulation that activates RNase L (Liu et al., 2019) (Figures S3B and S3C). Altogether, these results suggest that synthesized RNA circles display a stability similar to that of endogenous ones.

RNA circles produced from different *in vitro* strategies induce distinct immune responses

To test the immunogenic response of *in vitro* circularized RNAs produced by different strategies (Figure 1A), we measured mRNA levels of several inflammatory cytokines and innate immune regulators, including interferon (IFN) β ($IFN\beta$), tumor necrosis factor alpha ($TNF\alpha$), interleukin-6 ($IL-6$), and *RIG-I* after transfection of synthesized RNA circles.

We transfected the same amounts of exogenous *circPOLR2A* produced by methods I–III, poly(I:C) (widely used to mimic pathogenic dsRNAs), or different formats of linear *POLR2A* with the same sequences for circularization, individually, into A549 (human lung carcinoma) cells for 1 or 6 h. As expected, transfection of poly(I:C) or 5'-triphosphorylated linear *POLR2A* stimulated dramatic expression of examined inflammatory cytokines at 6 h, whereas moderate expression of these inflammatory cytokines was induced by transfection of dephosphorylated linear *POLR2A* (Figure 1C). Interestingly, transfection of *circPOLR2A_TD* and *circPOLR2A_Ana* also induced high-level expression of examined inflammatory factors that are comparable to dephosphorylated linear *POLR2A*, whereas transfection of *circPOLR2A_Lig* barely

induced expression of inflammatory cytokines and *RIG-I* (Figure 1C). The same immunogenic response assays were performed in HeLa and HEK293 cells and consistent results were observed (Figures S4A and S4B), except that some examined inflammatory cytokines were provoked at a lower level, i.e., *RIG-I* in HeLa cells. Thus, circular RNAs generated by autocatalytic introns could activate immune responses at a level comparable to that of dephosphorylated linear RNAs but are less immunogenic than classical pathogenic mimics like 5'-triphosphate-containing linear RNAs or poly(I:C).

We compared the immunogenic responses of *in vitro* circularized RNAs purified via high-performance liquid chromatography (HPLC) with the same experimental condition as previously reported (Chen et al., 2019; Wesselhoeft et al., 2019). HPLC resolved *circPOLR2A_Ana* and its linear products into different peaks (Figure 1D). Denaturing PAGE validation showed that peak 2 (fractions 5 and 6) from HPLC contains *circPOLR2A_Ana* without detectable linear products. HPLC-purified *circPOLR2A_Ana* also retained immune response, comparable to that purified by PAGE extraction and RNase R (Figure 1E). These results confirmed that circular *POLR2A* synthesized by method III can trigger expression of inflammatory cytokines.

Size exclusion chromatography appeared incapable of resolving *circPOLR2A_Lig* or *circPOLR2A_TD*, as shown by the observations that the gel-purified *circPOLR2A_Lig* or *circPOLR2A_TD* displayed a single HPLC peak, which was the same as the single HPLC peak of each corresponding purified linear RNA (Figures S4C and S4D). Nevertheless, such a double procedure (gel extraction plus HPLC) to purify *circPOLR2A_TD* induced expression of inflammatory cytokines, but *circPOLR2A_Lig* did not (data not shown).

Altogether, these results suggest that circular RNAs made by different *in vitro* circularization strategies can induce distinct innate immune responses. Specifically, circularized RNAs by direct ligation with T4 RNA ligase (method I) induced little immune response (5% to 10% compared with dephosphorylated linear RNAs), whereas circularized RNAs by self-splicing-dependent methods II and III provoked immune response with a comparable level to dephosphorylated linear RNAs in A549 cells (Figures 1C and 2A).

Circularized RNAs containing unwanted extra fragments (E1 + E2 + spacer) by autocatalytic splicing can induce immune responses

We set out to address how circular RNAs produced by methods II and III via permuted group I intron self-splicing for

(B) Different *circPOLR2A* circles containing exogenous fragments from *td* or pre-tRNA genes produced by method I show distinct immunogenicity. Left, schematic of method I was used to produce three types of *circPOLR2A* circles that harbor identical sequences, as illustrated in Figure 1A. Right, different *circPOLR2A* circles produced using direct ligation (method I) show distinct immunogenicity. Transfection of the same amounts (200 ng for each sample) of unmodified *circPOLR2A_TD_Lig* and *circPOLR2A_Ana_Lig* resulted in a comparable level of inflammatory cytokines to those by *circPOLR2A_TD* and *circPOLR2A_Ana* in A549 cells.

(C) Circular RNA with a complete reverse order produced via method I displays distinct immunogenicity. Left, three *circPOLR2A* with the same sequences as shown in Figure 1A were produced by method I in the reverse complementary orientation. Right, transfection of *circPOLR2A_TD* and *circPOLR2A_Ana* in the reverse complementary orientation of the same amount (200 ng for each sample) into A549 cells stimulated an innate immune response, but *circPOLR2A_Lig* in the reverse complementary orientation did not.

Relative expression of innate immune genes in A549 cells after 6 h of transfection are measured by qRT-PCR, with relative fold change normalized to expression of Ctrl (mock) transfection. Error bars represent SD. * $p < 0.05$, ** $p < 0.01$, *** $p < 0.001$, Student's t test.

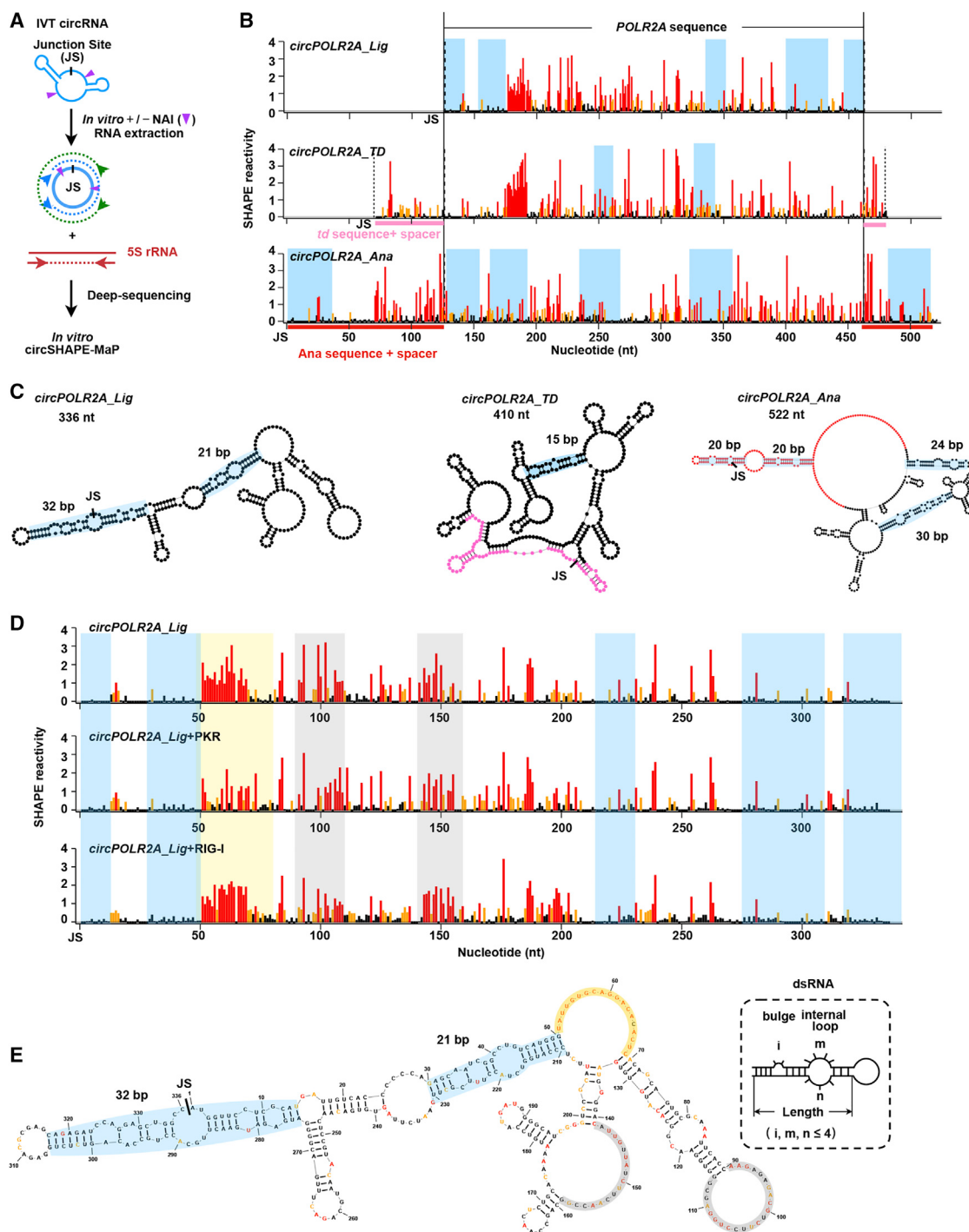


Figure 3. Circular RNAs synthesized by different circularization strategies have distinct structural conformations

(A) Illustration of *in vitro* circSHAPE-MaP assays of purified circular RNAs synthesized *in vitro* by the different circularization strategies shown in Figure 1A.

(B) CircSHAPE-MaP profiles of circPOLR2A_Lig, circPOLR2A_TD, and circPOLR2A_Ana. Pink and red lines indicate the extra fragments introduced by auto-catalytic splicing in circPOLR2A_TD and circPOLR2A_Ana.

(C) Predicted secondary structure models of circPOLR2A_Lig, circPOLR2A_TD, and circPOLR2A_Ana from *in vitro* circSHAPE-MaP. The imperfect short RNA duplexes of 16–33 bp in length are indicated in blue shadows. The short imperfect dsRNA duplex of circPOLR2A_TD is formed by a 15 nt single-stranded RNA (ssRNA) paired to a 16 nt ssRNA (blue shadow).

(legend continued on next page)

circularization could induce immune responses. First, to exclude any effect of the *POLR2A* sequences on the immunogenicity of circular RNAs, we applied the aforementioned three methods to generate *circmCherry_Lig*, *circmCherry_TD*, or *circmCherry_Ana*, all containing the same *mCherry* coding sequence that is not expressed in mammalian cells, as well as a coxsackievirus B3 internal ribosome entry site (CVB3 IRES) (Figure 2A, left panel; Figures S1B and S1C). After transfection, similar results were observed: *circmCherry_Lig* barely induced an innate immune response, whereas *circmCherry_TD* and *circmCherry_Ana* stimulated high-level expression of inflammatory cytokines in A549 cells (Figure 2A, right panels).

Next, we asked whether the immune responses observed in Figures 1C, 2A, S4A, and S4B by *circRNAs_TD* or *circRNAs_Ana* depended on circularization strategy. To answer this question, we directly ligated *in vitro* transcribed linear sequences for *circPOLR2A_TD* (named *circPOLR2A_TD_Lig*) and *circPOLR2A_Ana* (named *circPOLR2A_Ana_Lig*) with T4 RNA ligase (method I), which contain the additional 74 or 186 nt sequence (Figures 1A and S1A) in the final RNA circles, just like *circPOLR2A_TD* and *circPOLR2A_Ana* made by methods II and III (Figure 2B, left panel). Remarkably, transfection of *circPOLR2A_TD_Lig* and *circPOLR2A_Ana_Lig* into A549 cells led to comparable expression of examined inflammatory cytokines to those stimulated by *circPOLR2A_TD* and *circPOLR2A_Ana* (Figure 2B, right panels). These observations prompted us to conclude that the observed innate immune responses of *in vitro* circularized RNAs likely resulted from 74 and 186 nt extraneous sequences introduced into circular RNAs after self-splicing.

Third, to confirm effects of such exogenous sequence-mediated immune responses, we produced *circPOLR2A_Lig.RE*, *circPOLR2A_TD.RE*, and *circPOLR2A_Ana.RE* with REverse complementary sequences of *circPOLR2A_Lig*, *circPOLR2A_TD*, and *circPOLR2A_Ana* (Figure 2C, left panel) by T4 RNA ligase and transfected these two sets of circular RNAs (Figure 1A) into A549 cells for comparison. We reasoned that such a reverse complementary orientation would change the single-stranded sequence but largely preserve the overall RNA secondary structure (Fischer et al., 2020), including the 74 and 186 nt extra fragments (E1 + E2 + spacer). We observed that RNA circles with reverse complementary sequences (*circPOLR2A_TD.RE* and *circPOLR2A_Ana.RE*) were still capable of inducing high-level expression of inflammatory cytokines and RIG-I, whereas *circPOLR2A_Lig* and its reverse complement (*circPOLR2A_Lig.RE*) barely induced an immune response (Figure 2C, right panels).

Collectively, circular RNAs produced by T4 RNA ligase-based circularization (method I), which only introduces extra 1 to 3 nucleotides, avoid provoking innate immune responses, whereas group I intron autocatalytic splicing-based circularization (methods II and III) can stimulate immune responses because of the remnant extra nucleotides in the final circularized RNA

products, likely in a secondary structure-dependent manner. Alternatively, misfolded but partially flexible dsRNA segments are more immunogenic and have been observed for virus-associated (VA-I) RNA (Hood et al., 2019).

Remnant fragments (E1 + E2 + spacer) in circularized RNAs produced by autocatalytic splicing can trigger additional intramolecular RNA duplexes

How do circular RNAs produced by group I intron autocatalytic splicing induce immune response? One possibility is that the remnant fragments (E1, E2, and spacer) introduced by different types of group I intron autocatalytic splicing might have special topological structures that distinguish them from the RNA ligase-based circular RNAs, which would allow them to be recognized by nucleic acid receptors such as RIG-I.

We performed *in vitro* circSHAPE-MaP (selective 2'-hydroxyl acylation analyzed by primer extension and mutational profiling for circular RNAs) to compare circular RNAs produced by these different methods (Figure 3A). Such *in vitro* circSHAPE-MaP assays were optimized from our previously developed in cell circSHAPE-MaP (Guo et al., 2021; Liu et al., 2019). In brief, two sets of divergent primers crossing the ligation junction site (JS) were designed for each circular RNA. Two sets of RNA circles containing *POLR2A* or *CAMSAP1* by three methods (Figure 1A) were assayed, and SHAPE-MaP signals were generated for comparison (Figure S5A; Table S1). These two circular RNAs were chosen because their secondary structures in cells have been resolved (Liu et al., 2019).

Duplicate assays were performed with human 5S rRNA as an internal control (Figure S5A). NAI (2-methylnicotinic acid imidazolidine) probing *in vitro* gave rise to consistent and reliable signals for SHAPE-MaP assays with ~300 bp long tiling PCR products for each circular RNA, using *POLR2A* circles parallelly produced via different strategies as an example (Figure 3B). An in-house pipeline was developed to analyze *in vitro* SHAPE-MaP results (Guo et al., 2021). Examined structures of the spiked-in human 5S rRNA in circSHAPE-MaP duplicates were highly correlated and comparable to the reported 5S rRNA structure (Spitale et al., 2013) (Figure S5A), confirming that these independent SHAPE-MaP reactions were reliable for comparison among circular RNAs produced via methods I–III.

Conformational analysis revealed that *circPOLR2A_Lig*, *circPOLR2A_TD*, and *circPOLR2A_Ana* all formed one or two imperfect short RNA duplexes between 16 and 33 bp (blue shadow) within the corresponding *POLR2A* sequence (Figures 3C and S5B). We detected that E1, E2, and spacer fragments introduced by group I intron autocatalytic splicing tend to form additional and longer stem-loop regions (Figures 3C and S5B). Similar additional structural regions were found in *circCAMSAP1_TD* and *circCAMSAP1_Ana* (Figure S6A). Such structures formed within the circles are quite stable, which is

(D) Secondary structure models from *in vitro* circSHAPE-MaP reactivities for *circPOLR2A_Lig* (upper) supplemented with purified and dephosphorylated PKR proteins (middle) or RIG-I proteins (bottom). The yellow shadow denotes reduced SHAPE reactivities upon PKR addition; gray shadows denote unaltered high SHAPE reactivities upon PKR addition.

(E) Predicted secondary structure model of *circPOLR2A_Lig*, which contains two imperfect dsRNA modules (blue shadows, 32 and 21 bp). The heavy yellow line denotes the reduced SHAPE reactivities showing the altered single-stranded RNA region close to the imperfect dsRNA region upon PKR addition. Heavy gray lines denote the unaltered SHAPE reactivities showing the unaltered single-stranded RNA region upon PKR addition as controls.

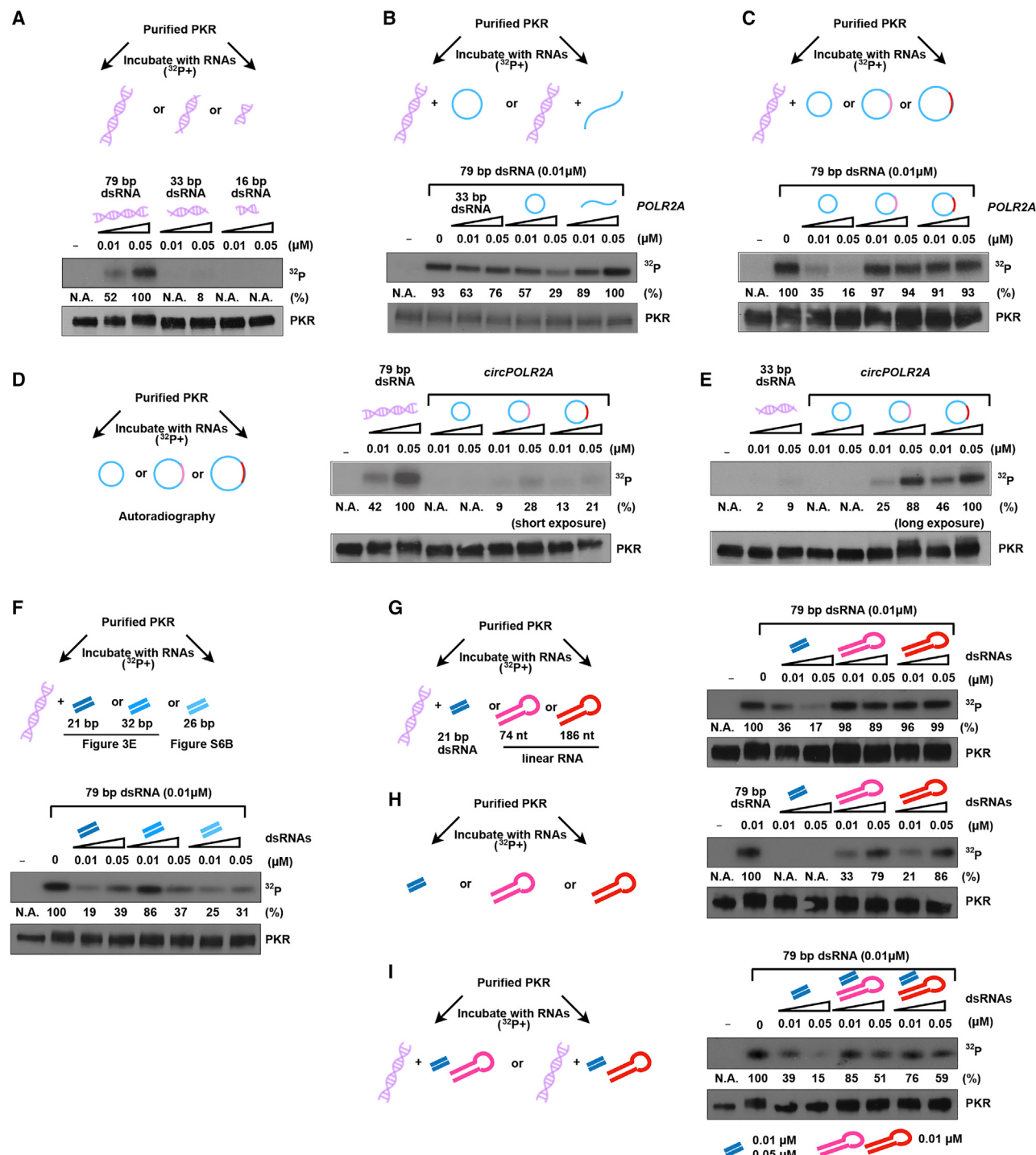


Figure 4. PKR recognizes dsRNA regions or exogenous sequences of circular RNAs produced by different strategies

(A) *In vitro* activation of PKR by dsRNAs with different lengths. *In vitro* activation assay of PKR (0.6 μM) induced by dsRNAs with different lengths and shown by autoradiography using $\gamma^{32}\text{P}$ -ATP. Concentrations of 16, 33, and 79 bp dsRNA are 0.01 and 0.05 μM .

(B) CircPOLR2A_Lig, but not its dephosphorylated linear cognate with the same sequence, inhibits PKR phosphorylation (p-PKR) *in vitro*. *In vitro* activation assay of PKR (0.6 μM) induced by 79 bp dsRNA (0.01 μM) and shown by autoradiography using $\gamma^{32}\text{P}$ -ATP.

(C) CircPOLR2A_Lig, but not circPOLR2A_TD and circPOLR2A_Ana, inhibits PKR phosphorylation *in vitro*.

(D) CircPOLR2A_TD and circPOLR2A_Ana activate PKR *in vitro*. PKR activation by circPOLR2A_TD and circPOLR2A_Ana was lower than 79 bp dsRNA at the same concentration.

(legend continued on next page)

supported by the notion that the SHAPE reactivities of these remnant E1, E2, and spacer fragments introduced after the group I intron autocatalytic reaction were similar (Spearman correlation > 0.9) yet were independent from the specific circular RNAs used for circularization (Figures S6B and S6C).

Analysis of circSHAPE-MaP data suggested that the 186 nt extraneous sequence from the Anabaena pre-tRNA group I autocatalytic intron could form an imperfect duplex longer than 50 bp in circularization of both *circPOLR2A_Ana* and *circCAMSAP1_Ana* (Figures 3B, 3C, and S6C). This imperfect duplex formed by the 186 nt of Anabaena pre-tRNA E1, E2, and spacer is strong, because *in silico* prediction of it led to almost the identical structure (Figure S6C). In contrast, the 74 nt fragment of E1, E2, and spacer from the *td* intron interacted with circular RNA sequences in *circPOLR2A_TD* (Figures 3B and 3C) or *circCAMSAP1_TD* (Figure S6A) and thus distorted the folding status of original circular RNAs. These interactions were different from *in silico* structure prediction of the 74 nt sequence that alone resulted in an imperfect dsRNA region (Figure S6B).

Collectively, these results indicate that the remnant fragments of E1, E2, and spacer in synthesized RNA circles via autosplicing (Figure 1A) tend to form stable intramolecular RNA duplexes, which likely lead to the observed immune responses after transfection. In contrast, *in vitro* circularized RNAs without these *td* or pre-tRNA gene fragments, such as *circPOLR2A_Lig* and *circmCherry_Lig*, induced minimized innate immune responses in transfected cells (Figures 1C, 2, S4A, and S4B).

RNA circles with minimized immunogenicity produced by T4 RNA ligase bind to PKR

Endogenously produced circRNAs as a group suppress PKR activation (Liu et al., 2019). After clarifying the immunogenicity of *in vitro* circularized RNAs (Figures 1, 2, 3, and S1–S6), we next explored the possibility of using RNA circles as novel types of PKR aptamers.

To better understand circular RNA-PKR interactions, we performed circSHAPE-MaP comparison of *circPOLR2A_Lig* with minimized cellular immunogenicity (Figures 1C, 2, and S4) and supplemented with purified and dephosphorylated PKR proteins (Figure S7C). Purified RIG-I was added as a control (Figure S7C). Remarkably, most nucleotides of *circPOLR2A_Lig* exhibited similar SHAPE reactivities before and after PKR addition except one single-stranded bulge region that is closely adjacent (yellow shadow, Figure 3D) to the imperfect 21 bp dsRNA region that potentially binds PKR. This observation makes sense, because the already-formed dsRNA region (blue shadow, Figure 3D) that

has low SHAPE reactivity would not display additional changes upon PKR binding, but PKR binding would influence NAI accessibility to the single-stranded region near its bound RNA duplexes, thereby altering SHAPE reactivities (Figure 3D). As controls, distal single-stranded regions showed little change in SHAPE reactivities after incubation with PKR (gray, Figures 3D and 3E). Addition of RIG-I did not result in measurable changes of SHAPE reactivities of *circPOLR2A_Lig*, including all detected single-stranded regions (Figure 3D). PKR binding to circular RNAs is structure dependent, because similar observations were found in *circCAMSAP1_Lig* (Figures S7A and S7B) and what we have previously shown using cellular assays (Liu et al., 2019). Moreover, the same immunogenic response assays of *circCAMSAP1* were performed in A549 cells, and consistent results were observed (Figure S7D).

CircPOLR2A_Lig, but not circPOLR2A_TD and circPOLR2A_Ana, prevents PKR activation *in vitro*

PKR is an IFN-inducible Ser/Thr protein kinase that is directly activated by long dsRNA (>33 bp, with 79 bp achieving maximal activation) and plays a central role in the innate immune response to dsRNAs, whereas short dsRNAs of 16–33 bp in length can bind PKR monomers and block activation *in vitro* (Bou-Nader et al., 2019; Nallagatla et al., 2011; Zheng and Bevilacqua, 2004). Given that *in vitro* synthesized *circPOLR2A_Lig* also formed 21 and 32 bp imperfect short RNA duplexes (Figure 3C), we examined whether adding synthesized *circPOLR2A_Lig* could prevent PKR activation, using its 5'-dephosphorylated cognate linear *POLR2A* with the same sequence as a control.

PKR was obtained by histidine-tagged affinity purification and further dephosphorylated by λ-phosphatase (Figure S7C). Consistent with previous studies (Liu et al., 2019), incubation of 79 bp dsRNAs (0.01 μM), but not 33 or 16 bp dsRNAs, with PKR (0.6 μM) dramatically induced PKR phosphorylation *in vitro* (Figure 4A). Addition of the same or five-fold amount of 33 bp dsRNAs to the 79 bp dsRNA-activated PKR blocked activation (Figure 4B). Furthermore, addition of purified *circPOLR2A_Lig*, but not the 5'-dephosphorylated linear *POLR2A* with the same sequence, repressed PKR activation (Figure 4B). Compared with *circPOLR2A_Lig*, adding the same amount of *circPOLR2A_TD* or *circPOLR2A_Ana* did not suppress PKR activation (Figure 4C).

Instead, *circPOLR2A_TD* or *circPOLR2A_Ana* alone could induce PKR activation to a level that was weaker than 79 bp dsRNAs (short exposure, Figure 4D) but much higher than 33 bp dsRNAs (long exposure, Figure 4E). As a control,

(E) CircPOLR2A_TD and circPOLR2A_Ana activate PKR *in vitro*. PKR activation by *circPOLR2A_TD* and *circPOLR2A_Ana* was higher than 33 bp dsRNA at the same concentration.

(F) Dephosphorylated, imperfect dsRNAs (21, 32, and 26 bp) from *in vitro*-made circles *circPOLR2A_Lig* (Figure 3E) and *circCAMSAP1_Lig* (Figure S6B) inhibit PKR phosphorylation *in vitro*.

(G) Dephosphorylated imperfect 21 bp dsRNA, but not the 74 or 186 nt extraneous fragments introduced by group I intron autocatalytic splicing, inhibits PKR phosphorylation *in vitro*.

(H) 74 or 186 nt extraneous fragments introduced by group I intron splicing alone activate PKR phosphorylation *in vitro*, but to a less efficient level than the 79 bp dsRNA.

(I) Competitive *in vitro* PKR activation assays show that 74 and 186 nt extraneous fragments dampen the inhibitory effect of the 21 bp imperfect short RNA duplexes from *circPOLR2A_Lig* on PKR activation.

Experiments were independently repeated, and similar results were observed. The *in vitro* PKR activation assay was performed as shown in (A). The level of p-PKR in each representative experiment was quantified by Quantity One, and p-PKR levels were normalized by PKR expression.

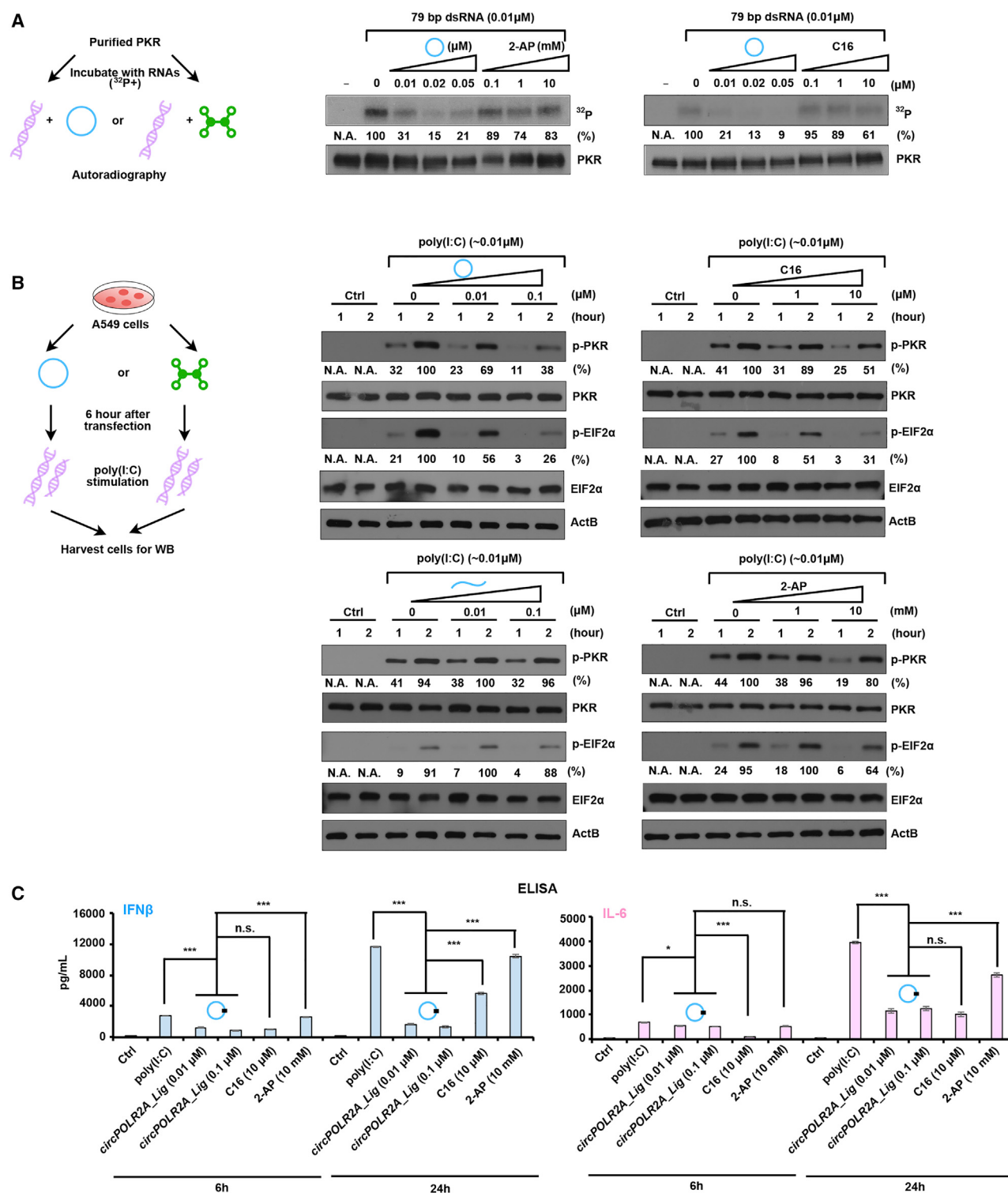


Figure 5. CircPOLR2A_Lig efficiently prevents PKR activation *in vitro* and in cells

(A) CircPOLR2A_Lig suppresses PKR phosphorylation with dramatically higher efficiency than 2-AP or C16 *in vitro*. PKR (0.6 μM) activation induced by 79 bp dsRNA and shown by autoradiography using $\gamma^{32}\text{P}$ -ATP is blocked by addition of circPOLR2A_Lig, 2-AP, or C16 *in vitro*.

(B) CircPOLR2A_Lig suppresses PKR phosphorylation and downstream eIF2 α phosphorylation with dramatically higher efficiency than 2-AP or C16 in cells. A549 cells transfected with circPOLR2A_Lig or added PKR inhibitors into cell culture medium at the indicated concentrations for 6 h, followed by poly(I:C) treatment at

(legend continued on next page)

Molecular Cell

Article



circPOLR2A_Lig did not induce detectable PKR activation (Figures 4D and 4E). These results were in line with the identified immunogenicity of *in vitro* circularized RNAs that contain extraneous E1, E2, and spacer fragments (Figures 1 and 2).

To narrow down the effective duplex regions that suppress PKR activation in *circPOLR2A_Lig* (Figure 3E) and *circCAMSAP1_Lig* (Figure S7B), we generated imperfect dephosphorylated dsRNAs with lengths of 21 and 32 bp in *circPOLR2A_Lig* (Figure 3E) and 26 bp in *circCAMSAP1_Lig* (Figure S7B) identified in these *in vitro*-made circles for analysis. As expected, addition of these imperfect short duplexes successfully suppressed PKR activation *in vitro* (Figure 4F, bottom panel). We also synthesized and purified the linear 74 and 186 nt extraneous fragments introduced by group I intron self-splicing (Figure 4G, left panel), followed by dephosphorylation and refolding. These sequences tend to form long (35 and >50 bp, respectively) RNA duplexes (Figures S6B and S6C). As expected, adding these fragments did not block PKR phosphorylation by 79 bp dsRNAs (Figure 4G, right panel); instead, these fragments alone induced PKR activation (Figure 4H). Importantly, competition assays revealed both 74 and 186 nt fragments dampened the inhibitory effect of the imperfect short RNA duplexes from *circPOLR2A_Lig* (Figure 4I). Similar dampened inhibitory effects were observed by *circPOLR2A_TD* and *circPOLR2A_Ana* (Figure S8). Thus, it appeared that the stimulatory 74 and 186 nt fragments introduced by the autolytic splicing in RNA circles were dominant over the imperfect, inhibitory short RNA duplexes formed in the same circular RNAs on PKR activation (Figure S8). These results were consistent with the observation that *circPOLR2A_TD* and *circPOLR2A_Ana* could not repress PKR activation, even though they have the imperfect short RNA duplexes between 16 and 33 bp (Figure 4C).

Collectively, the observations that *circPOLR2A_Lig* can avoid provoking innate immune responses (Figures 1C, 1E, 2, S4A, and S4B) and inhibit PKR activation *in vitro* (Figure 4) strongly suggest that *circPOLR2A_Lig* and other circular RNAs containing short dsRNA regions, such as *circCAMSAP1_Lig*, are promising for therapeutic application to dampen PKR activity compared with *circPOLR2A_TD* and *circPOLR2A_Ana*.

CircPOLR2A_Lig prevents PKR activation *in vitro* and in cells dramatically more effectively than chemical compounds

Finally, we assessed the inhibitory effect of *circPOLR2A_Lig* on PKR activation compared with commercially available small molecular PKR inhibitors. For example, 2-aminopurine (2-AP) is an inhibitor of PKR activity at millimolar concentrations and has been long used to inhibit PKR in cells (Huang and Schneider, 1990). Another broadly used PKR inhibitor is the imidazole/oxindole-derived inhibitor of PKR compound #16 (C16), which was discovered by screening a library of 26 ATP binding site-directed inhibitors of varying structures (Jammi et al., 2003).

the indicated time points. PKR phosphorylation (p-PKR-T446, p-PKR for simplicity), eIF2 α phosphorylation (p-eIF2 α -S51, p-eIF2 α for simplicity), PKR expression, and eIF2 α expression were assayed.

Experiments were independently repeated, and similar results were observed. The level of p-PKR and p-eIF2 α in each panel was quantified by Quantity One, and p-PKR or p-eIF2 α levels were normalized by PKR or eIF2 α expression, respectively.

(C) *CircPOLR2A_Lig* prevents the production of IFN β and IL-6 stimulated by poly(I:C) in A549 cells, as shown by ELISA. Error bars represent SD. n.s. (non-significant), p > 0.05, *p < 0.05, **p < 0.001, Student's t test.

To compare the inhibitory effects of *circPOLR2A_Lig* to 2-AP or C16 on PKR activation, we performed *in vitro* PKR (0.6 μ M) activity assays stimulated by the 79 bp dsRNAs (0.01 μ M). PKR activation was shown by autoradiography using γ -³²P-ATP (10 μ Ci per reaction). Strikingly, *circPOLR2A_Lig* inhibited PKR phosphorylation more effectively (10⁶- or 10³-fold higher) than 2-AP (up to 10 mM) or C16 (up to 10 μ M) did *in vitro* (Figure 5A). Similarly, we observed stronger inhibitory effects of *circPOLR2A_Lig* than of 2-AP or C16 on PKR and downstream α subunit of the eukaryotic initiation factor (eIF2 α) activation in cells upon poly(I:C) stimulation (Figure 5B), whereas the dephosphorylated linear POLR2A had no inhibitory effect (Figure 5B). Enzyme-linked immunosorbent assay (ELISA) using cell culture supernatant stimulated by poly(I:C) for 6 and 24 h also showed that *circPOLR2A_Lig* prevented the production of downstream cytokine proteins (IFN β and IL-6). *CircPOLR2A_Lig* (0.01 to ~0.1 μ M) displayed a comparable inhibitory effect compared with C16 (10 μ M) upon poly(I:C) stimulation at 6 h and a stronger inhibitory effect at 24 h on examined IFN β . The inhibitory effects of 2-AP (10 mM) on downstream cytokine protein production were barely detected (Figure 5C).

Because C16 was previously reported to suppress proliferation of hepatocellular carcinoma (HCC) cells in a dose-dependent manner (Watanabe et al., 2020), we examined whether *circPOLR2A_Lig* transfection would cause side effects such as with C16. Cell proliferation assays revealed that although C16 suppressed A549 proliferation as reported, *circPOLR2A_Lig* transfection barely influenced cell proliferation (Figure S9A). However, consistent with the important role of PKR in innate immunity, transfection of *circPOLR2A_Lig* (0.1 μ M) facilitated encephalomyocarditis (EMCV) replication with a comparable level to C16 (10 μ M) and 2-AP (10 mM) in A549 cells (Figure S9B).

Finally, it was shown that IFN γ treatment can induce PKR activation via the PKR activating protein (PACT)-mediated signaling pathway (Patel and Sen, 1998). We found that *circPOLR2A_Lig* at the same concentration that was used to suppress poly(I:C)-activated PKR (Figure 5) did not suppress IFN γ -induced PKR activation (Figure 6A). PKR-PACT interaction depends on the M1 and M2 domains of PACT (Figure S9D), as previously reported (Chukwurah et al., 2018). Consistent with the results shown in Figure 6A, addition of *circPOLR2A_Lig* did not affect interactions between PKR and PACT, or those between PKR and truncated PACTs, before or after IFN γ stimulation (Figures 6B and S9D), indicating that *circPOLR2A_Lig* cannot inhibit PACT-mediated PKR activation when treated with IFN γ . These observations suggest that *circPOLR2A_Lig* preferred to suppress the activation of PKR using long dsRNAs (Figures 4, 5, and 6).

DISCUSSION

Endogenous circRNAs produced from back-splicing are covalently closed, single-stranded RNA species. They are stable

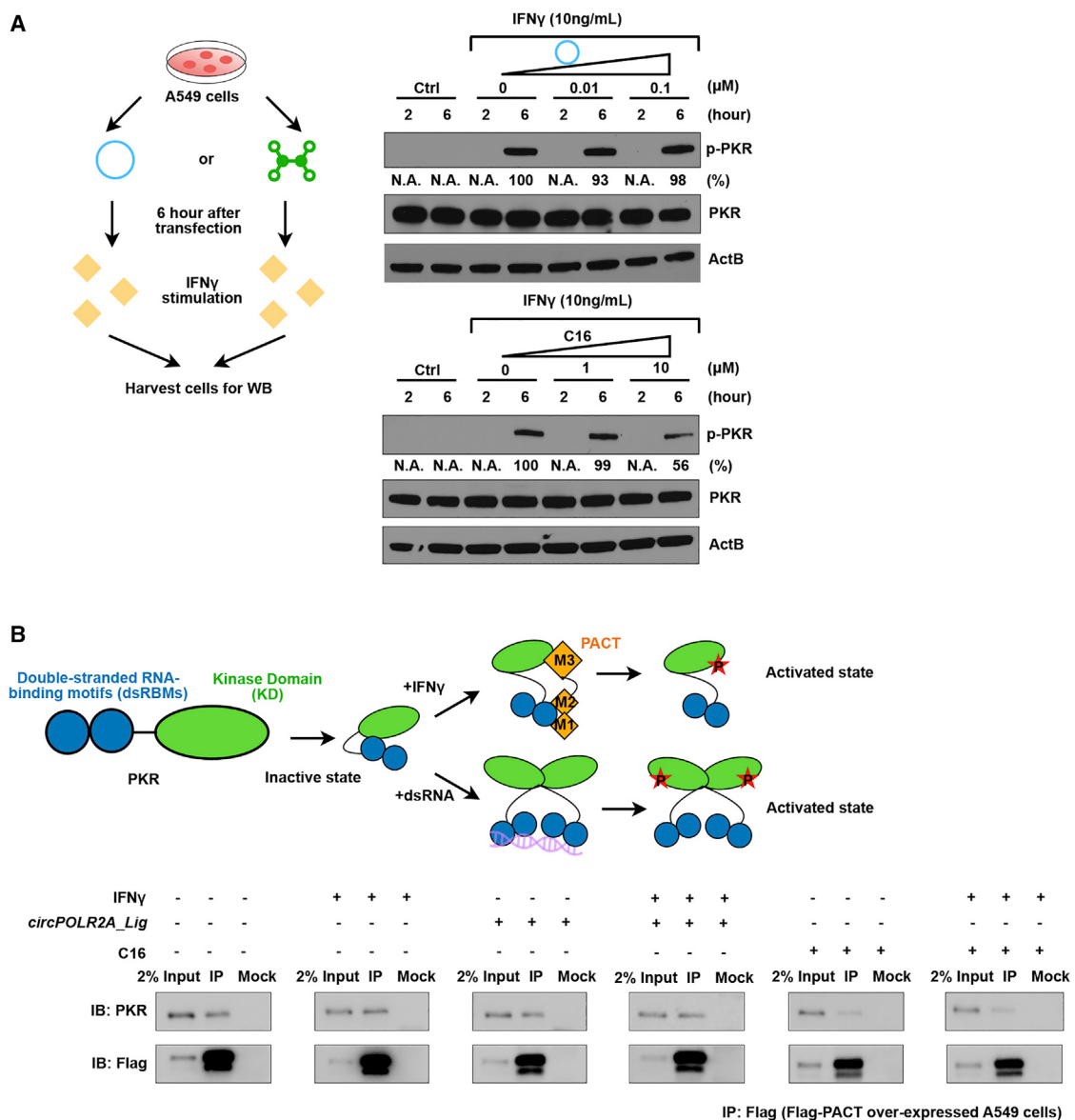


Figure 6. CircPOLR2A_Lig did not suppress IFN γ -induced PKR activation

(A) CircPOLR2A_Lig does not suppress IFN γ -induced PKR phosphorylation in cells. A549 cells were transfected with CircPOLR2A_Lig or added C16 to the cell culture at the indicated concentrations for 6 h, followed by IFN γ treatment at the indicated time points and the detection of p-PKR. Experiments were independently repeated, and similar results were observed. The level of p-PKR in each panel was quantified by Quantity One, and p-PKR levels were normalized by PKR expression.

(B) CircPOLR2A_Lig has no detectable effect on PKR-PACT binding before or after IFN γ stimulation. Top, illustration shows that PACT binds PKR, leading to PKR activation (upper), whereas RNA circles interact with dsRNA binding motifs (dsRBMs) of PKR to prevent its activation without interfering with the kinase domain of PKR (lower). Bottom, FLAG-PACT overexpressed A549 cells were generated and followed by immunoprecipitation (IP) to examine PKR-PACT interaction. CircPOLR2A_Lig did not affect PKR-PACT binding before or after IFN γ stimulation. In contrast, the addition of C16, which was known to block the ATP binding site of the kinase domain for PKR phosphorylation (Jammie et al., 2003) led to decreased PKR-PACT binding before and after IFN γ stimulation. Experiments were independently repeated, and similar results were observed.

(Enuka et al., 2016; Zhang et al., 2016a) and short circRNAs have unique structural conformations (Fischer et al., 2020; Liu et al., 2019) that are distinct from linear RNAs. Their unique biogenesis and structure have endowed them with previously underappreciated applications in biomedical research. For example, *in vitro* synthesis of immunogenicity-free circular RNAs has potential

for the development of novel aptamers to dampen autoimmune-disease-related PKR activation (Liu et al., 2019) or to be used as RNA vehicles for translation with engineered IRESs (Wesselhoeft et al., 2018, 2019).

Here, we report that *in vitro* synthesized CircPOLR2A_Lig by T4 RNA ligase (method I, Figure 1A) successfully yields

Molecular Cell

Article



minimized immunogenicity (**Figures 1C, 2, and S4**) and short dsRNA-containing (**Figures 3C, 3E, 3G, S5, and S7**) RNA circles as effective PKR inhibitors (**Figures 4 and 5**). *CircPOLR2A_Lig* displayed significantly higher suppressive effects on PKR activation *in vitro* and in cells than the commonly used PKR inhibitors C16 and 2-AP (**Figure 5**), with little cellular toxicity (**Figure S9A**). We also investigated additional RNA inhibitors of PKR, including VA-1 ([Mathews and Shenk, 1991](#)) and the human noncoding RNA 886 (*nc886*) ([Fort et al., 2018; Lee et al., 2016, 2011](#)). Although VA-1 and *nc886* showed comparable levels of inhibitory effects on PKR activation to *circPOLR2A_Lig* (**Figure S9C**), they both induced expression of inflammatory cytokines that was comparable to dephosphorylated linear *POLR2A* (**Figure S9C**). These results suggest the advantage of using circular nucleotide aptamers in dampening the activity of an enzyme that does not have critical docking sites with substrates while maintaining the minimized immunogenicity. It will be of importance to optimize even smaller and more effective circle aptamers to suppress PKR activation. In addition, because this direct ligation method is more efficient for the synthesis of shorter RNA circles (<500 nt) than longer ones (such as >1,000 nt) (**Figure S1**), optimization is needed to produce larger RNA circles with minimized immunogenicity.

In vitro circularized RNAs with methods II and III (**Figure 1A**) that use group I introns for self-splicing seem to be immunogenic. The identified immunogenicity of unmodified circular RNAs produced from self-splicing of the group I intron of the T4 phage *td* gene (method II, **Figure 1A**) was in line with previous findings ([Chen et al., 2017, 2019](#)); however, circularized RNAs produced by self-splicing of the Anabaena pre-tRNA group I intron (method III, **Figure 1A**) were reported to be immunogenicity free ([Wesselhoeft et al., 2019](#)). Detailed analyses of circularized RNAs produced from these two types of group I catalytic introns suggest that these RNA circles were indeed both capable of inducing cellular immune responses (**Figures 1C, 2, and S4**), which were comparable to phosphatase-treated linear RNAs but less immunogenic than 5'-triphosphate-containing linear RNAs (**Figures 1C, 2A, and S4**) ([Chen et al., 2017, 2019](#)). Multiple factors might contribute to the observed immunogenicity for RNA circles generated by group I intron self-splicing. For example, extraneous fragments of *td* and pre-tRNA genes in the final circular RNA products might trigger immune responses. Although a detailed mechanism remains elusive, the conformational changes rendered by these extraneous sequences might contribute to their immune responses (**Figures 3 and S6**). Such sequences alone appeared to stimulate PKR activation (**Figures 4G and 4H**), and were dominant over the inhibitory short RNA duplexes in the same RNA circles (**Figure S8**). Because the *td* intron-synthesized circular RNAs could be sensed by RIG-I ([Chen et al., 2017, 2019](#)), mechanisms of how circularized RNAs carrying these extraneous sequences could provoke immune responses are complicated and warrant future study.

In addition to differences in sequences, lengths, and shapes of RNA circles that might contribute to some distinct findings between this study and [Wesselhoeft et al. \(2019\)](#), the fg (femtogram) level of contaminating 5'-triphosphate linear RNAs might activate immune responses. This explained why RNA circles produced by

direct ligation with T4 RNA ligase also resulted in minimized expression of immune stimulatory genes (5% to 10%, compared with dephosphorylated linear RNAs) (**Figures 1C, 1E, and 2A**). Given the fg level of contaminating RNAs below the radar of detection by HPLC, PAGE, or other detectors, one cannot exclude that such contaminations may induce immune responses.

Nonetheless, because one possible application of *in vitro* circularized RNAs is to be used as a template for protein translation, whether engineered exogenous IRES sequences within circularized RNAs form strong structures to cause immune responses should be carefully evaluated case by case. For example, [Chen et al. \(2017, 2019\)](#) used an oligonucleotide-splinting ligation with T4 DNA ligase to create IRES-containing circular RNAs without the self-splicing intron, which was still immunogenic. In this case, using an oligonucleotide to splint the ligation junction could create more dsRNA structures, and the IRES (which is different from *circmCherry_Lig* in this study) (**Figure 2A**) in this particular RNA circle might add more structured regions that could potentially stimulate immune responses.

Collectively, circular RNAs are distinct from previously dominantly studied mRNAs and microRNAs (miRNAs), but they possess unique features that other types of RNAs do not have. Engineered circular RNAs *in vitro* have the potential for multiple biomedical applications, but their features should be carefully examined, given that different *in vitro* circularization methods may cause different conformations and immunogenicity.

Limitations of the study

Several unanswered questions at this stage warrant future study. First, although we were able to make RNA circles with minimized immunogenicity as potent PKR inhibitors, how the extraneous fragments of *td* and pre-tRNA genes in the final circular RNA products could provoke immune responses has remained elusive. Different immune response pathways, such as RIG-I ([Chen et al., 2017, 2019](#)) and PKR (**Figure S8**), may coordinately respond to these autolytic splicing-produced RNA circles to induce an immune response. Cellular immune responses to circular RNAs with different lengths and shapes produced by different approaches in different cell lines and *in vivo* should be tested. Second, we have shown that these extraneous fragments could form complicated three-dimensional structures (**Figures 3 and S5–S7**). Better understanding of their folding status, as well as the tertiary structure of each type of circular RNA made by different methods, will likely bring new insights into how they would interact with different RNA sensors. Third, given the high yields of using permuted phage *td* and pre-tRNA group I intron genes in synthesizing circular RNA *in vitro* (**Figures S1 and S2**), it will be of great interest to improve these strategies by reducing the immunogenicity of produced RNA circles for potential biomedical implications in both inhibitory and translational modes.

STAR★METHODS

Detailed methods are provided in the online version of this paper and include the following:

- KEY RESOURCES TABLE

- RESOURCE AVAILABILITY
 - Lead contact
 - Materials availability
 - Data and code availability
- EXPERIMENTAL MODEL AND SUBJECT DETAILS
 - Human cell lines
 - Cell culture, transfection and stimulation
 - Bacterial strains
- METHOD DETAILS
 - Plasmid construction
 - RNA isolation, RT-PCR, qRT-PCR and Northern Blotting (NB)
 - In vitro RNA transcription, circularization and purification
 - High Performance Liquid Chromatography (HPLC)
 - Protein expression and purification
 - In vitro activation assay of PKR
 - Enzyme-linked immunosorbent assay (ELISA)
 - Cell proliferation assay
 - In vitro SHAPE probing (with/without proteins)
 - SHAPE-MaP reverse transcription
 - SHAPE-MaP library preparation and sequencing
 - Co-Immunoprecipitation (IP)
- QUANTIFICATION AND STATISTICAL ANALYSIS
 - CircSHAPE-MaP data analyses
 - circRNA secondary structure modeling
 - Statistical analysis

SUPPLEMENTAL INFORMATION

Supplemental information can be found online at <https://doi.org/10.1016/j.molcel.2021.11.019>.

ACKNOWLEDGMENTS

We thank J. Zhang at NIH, H.Y. Chang at Stanford University, D.G. Anderson at MIT for comments, and the Chen lab members for discussion. This work was supported by the National Natural Science Foundation of China (NSFC) (91940303, 31725009, and 31821004), the National Key R&D Program of China (2021YFA1300501), the CAS Project for Young Scientists in Basic Research (YSBR-009), the Center for Excellence in Molecular Cell Science (CEMCS) (2020DF03), and the HHMI International Program (55008728) to L.-L.C.; the NSFC (31730111, 31925011, and 91940306) to L.Y.; and the China Postdoctoral Science Foundation (CPHF) (Y949603101) and NSFC (32000912) to C.-X.L. L.-L.C. acknowledges support from the Xplorer Prize.

AUTHOR CONTRIBUTIONS

L.-L.C. conceived the project. C.-X.L., S.-K.G., and Y.-F.X. performed experiments. F.N. and L.Y. preformed computational analyses. L.-L.C., C.-X.L., and S.-K.G. wrote the paper, with input from all authors. L.-L.C. supervised the project.

DECLARATION OF INTERESTS

L.-L.C., C.-X.L., S.-K.G., and Y.-F.X. are named as inventors on patents related to circular RNA held by the CAS CEMCS. L.-L.C. is a member of the Molecular Cell advisory board.

Received: April 5, 2021

Revised: August 31, 2021

Accepted: November 17, 2021

Published: December 23, 2021

REFERENCES

- Bou-Nader, C., Gordon, J.M., Henderson, F.E., and Zhang, J. (2019). The search for a PKR code-differential regulation of protein kinase R activity by diverse RNA and protein regulators. *RNA* 25, 539–556.
- Chen, L.L. (2020). The expanding regulatory mechanisms and cellular functions of circular RNAs. *Nat. Rev. Mol. Cell Biol.* 21, 475–490.
- Chen, Y.G., Kim, M.V., Chen, X., Batista, P.J., Aoyama, S., Wilusz, J.E., Iwasaki, A., and Chang, H.Y. (2017). Sensing Self and Foreign Circular RNAs by Intron Identity. *Mol. Cell* 67, 228–238.e5.
- Chen, Y.G., Chen, R., Ahmad, S., Verma, R., Kasturi, S.P., Amaya, L., Broughton, J.P., Kim, J., Cadena, C., Pulendran, B., et al. (2019). N6-Methyladenosine Modification Controls Circular RNA Immunity. *Mol. Cell* 76, 96–109.e9.
- Chukwurah, E., Willingham, V., Singh, M., Castillo-Azofeifa, D., and Patel, R.C. (2018). Contribution of the two dsRBM motifs to the double-stranded RNA binding and protein interactions of PACT. *J. Cell. Biochem.* 119, 3598–3607.
- Enuka, Y., Lauriola, M., Feldman, M.E., Sas-Chen, A., Ulitsky, I., and Yarden, Y. (2016). Circular RNAs are long-lived and display only minimal early alterations in response to a growth factor. *Nucleic Acids Res.* 44, 1370–1383.
- Fischer, J.W., Busa, V.F., Shao, Y., and Leung, A.K.L. (2020). Structure-Mediated RNA Decay by UPF1 and G3BP1. *Mol. Cell* 78, 70–84.e6.
- Fort, R.S., Mathó, C., Geraldo, M.V., Ottati, M.C., Yamashita, A.S., Saito, K.C., Leite, K.R.M., Méndez, M., Maedo, N., Méndez, L., et al. (2018). Nc886 is epigenetically repressed in prostate cancer and acts as a tumor suppressor through the inhibition of cell growth. *BMC Cancer* 18, 127.
- Gholamalipour, Y., Johnson, W.C., and Martin, C.T. (2019). Efficient inhibition of RNA self-primed extension by addition of competing 3'-capture DNA-improved RNA synthesis by T7 RNA polymerase. *Nucleic Acids Res.* 47, e118.
- Guo, S.K., Nan, F., Liu, C.X., Yang, L., and Chen, L.L. (2021). Mapping circular RNA structures in living cells by SHAPE-MaP. *Methods*. Published online February 9, 2021. <https://doi.org/10.1016/j.ymeth.2021.01.011>.
- Hood, I.V., Gordon, J.M., Bou-Nader, C., Henderson, F.E., Bahmanjeh, S., and Zhang, J. (2019). Crystal structure of an adenovirus virus-associated RNA. *Nat. Commun.* 10, 2871.
- Hornung, V., Ellegast, J., Kim, S., Brzózka, K., Jung, A., Kato, H., Poeck, H., Akira, S., Conzelmann, K.K., Schlee, M., et al. (2006). 5'-Triphosphate RNA is the ligand for RIG-I. *Science* 314, 994–997.
- Huang, J.T., and Schneider, R.J. (1990). Adenovirus inhibition of cellular protein synthesis is prevented by the drug 2-aminopurine. *Proc. Natl. Acad. Sci. USA* 87, 7115–7119.
- Jammi, N.V., Whitby, L.R., and Beal, P.A. (2003). Small molecule inhibitors of the RNA-dependent protein kinase. *Biochem. Biophys. Res. Commun.* 308, 50–57.
- Langmead, B., and Salzberg, S.L. (2012). Fast gapped-read alignment with Bowtie 2. *Nat. Methods* 9, 357–359.
- Lee, K., Kunkeaw, N., Jeon, S.H., Lee, I., Johnson, B.H., Kang, G.Y., Bang, J.Y., Park, H.S., Leelayuwat, C., and Lee, Y.S. (2011). Precursor miR-886, a novel noncoding RNA repressed in cancer, associates with PKR and modulates its activity. *RNA* 17, 1076–1089.
- Lee, E.K., Hong, S.H., Shin, S., Lee, H.S., Lee, J.S., Park, E.J., Choi, S.S., Min, J.W., Park, D., Hwang, J.A., et al. (2016). nc886, a non-coding RNA and suppressor of PKR, exerts an oncogenic function in thyroid cancer. *Oncotarget* 7, 75000–75012.
- Li, X., et al. (2017). Coordinated circRNA Biogenesis and Function with NF90/NF110 in Viral Infection. *Mol. Cell* 67, 214–227. <https://doi.org/10.1016/j.molcel.2017.05.023>.
- Liu, C.X., Li, X., Nan, F., Jiang, S., Gao, X., Guo, S.K., Xue, W., Cui, Y., Dong, K., Ding, H., et al. (2019). Structure and Degradation of Circular RNAs Regulate PKR Activation in Innate Immunity. *Cell* 177, 865–880.e21.
- Lorenz, R., Bernhart, S.H., Höner Zu Siederdissen, C., Tafer, H., Flamm, C., Stadler, P.F., and Hofacker, I.L. (2011). ViennaRNA Package 2.0. *Algorithms Mol. Biol.* 6, 26.

Molecular Cell

Article



- Mathews, M.B., and Shenk, T. (1991). Adenovirus virus-associated RNA and translation control. *J. Virol.* 65, 5657–5662.
- Matsui, T., Tanihara, K., and Date, T. (2001). Expression of unphosphorylated form of human double-stranded RNA-activated protein kinase in *Escherichia coli*. *Biochem. Biophys. Res. Commun.* 284, 798–807.
- Moffat, J., Grueneberg, D.A., Yang, X., Kim, S.Y., Kloepfer, A.M., Hinkle, G., Pigan, B., Eisenhaure, T.M., Luo, B., Grenier, J.K., et al. (2006). A lentiviral RNAi library for human and mouse genes applied to an arrayed viral high-content screen. *Cell* 124, 1283–1298.
- Moldovan, L.I., Hansen, T.B., Venø, M.T., Okholm, T.L.H., Andersen, T.L., Hager, H., Iversen, L., Kjems, J., Johansen, C., and Kristensen, L.S. (2019). High-throughput RNA sequencing from paired lesional- and non-lesional skin reveals major alterations in the psoriasis circRNAome. *BMC Med. Genomics* 12, 174.
- Moldovan, L.I., Tsoi, L.C., Ranjitha, U., Hager, H., Weidinger, S., Gudjonsson, J.E., Kjems, J., and Kristensen, L.S. (2021). Characterization of circular RNA transcriptomes in psoriasis and atopic dermatitis reveals disease-specific expression profiles. *Exp. Dermatol.* 30, 1187–1196.
- Nallagatla, S.R., Toroney, R., and Bevilacqua, P.C. (2011). Regulation of innate immunity through RNA structure and the protein kinase PKR. *Curr. Opin. Struct. Biol.* 21, 119–127.
- Patel, R.C., and Sen, G.C. (1998). PACT, a protein activator of the interferon-induced protein kinase, PKR. *EMBO J.* 17, 4379–4390.
- Reikine, S., Nguyen, J.B., and Modis, Y. (2014). Pattern Recognition and Signaling Mechanisms of RIG-I and MDA5. *Front. Immunol.* 5, 342.
- Safran, S.A., Eckert, D.M., Leslie, E.A., and Bass, B.L. (2019). PKR activation by noncanonical ligands: a 5'-triphosphate requirement versus antisense contamination. *RNA* 25, 1192–1201.
- Schindewolf, C., Braun, S., and Domdey, H. (1996). *In vitro* generation of a circular exon from a linear pre-mRNA transcript. *Nucleic Acids Res.* 24, 1260–1266.
- Schlee, M., and Hartmann, G. (2016). Discriminating self from non-self in nucleic acid sensing. *Nat. Rev. Immunol.* 16, 566–580.
- Smola, M.J., Rice, G.M., Busan, S., Siegfried, N.A., and Weeks, K.M. (2015). Selective 2'-hydroxyl acylation analyzed by primer extension and mutational profiling (SHAPE-MaP) for direct, versatile and accurate RNA structure analysis. *Nat. Protoc.* 10, 1643–1669.
- Spitale, R.C., Crisalli, P., Flynn, R.A., Torre, E.A., Kool, E.T., and Chang, H.Y. (2013). RNA SHAPE analysis in living cells. *Nat. Chem. Biol.* 9, 18–20.
- Warren, L., Manos, P.D., Ahfeldt, T., Loh, Y.H., Li, H., Lau, F., Ebina, W., Mandal, P.K., Smith, Z.D., Meissner, A., et al. (2010). Highly efficient reprogramming to pluripotency and directed differentiation of human cells with synthetic modified mRNA. *Cell Stem Cell* 7, 618–630.
- Watanabe, T., Ninomiya, H., Saitou, T., Takanezawa, S., Yamamoto, S., Imai, Y., Yoshida, O., Kawakami, R., Hirooka, M., Abe, M., et al. (2020). Therapeutic effects of the PKR inhibitor C16 suppressing tumor proliferation and angiogenesis in hepatocellular carcinoma *in vitro* and *in vivo*. *Sci. Rep.* 10, 5133.
- Wesselhoeft, R.A., Kowalski, P.S., and Anderson, D.G. (2018). Engineering circular RNA for potent and stable translation in eukaryotic cells. *Nat. Commun.* 9, 2629.
- Wesselhoeft, R.A., Kowalski, P.S., Parker-Hale, F.C., Huang, Y., Bisaria, N., and Anderson, D.G. (2019). RNA Circularization Diminishes Immunogenicity and Can Extend Translation Duration *In Vivo*. *Mol. Cell* 74, 508–520.e4.
- Xiao, M.S., Ai, Y., and Wilusz, J.E. (2020). Biogenesis and Functions of Circular RNAs Come into Focus. *Trends Cell Biol.* 30, 226–240.
- Zhang, X.O., Wang, H.B., Zhang, Y., Lu, X., Chen, L.L., and Yang, L. (2014). Complementary sequence-mediated exon circularization. *Cell* 159, 134–147.
- Zhang, Y., Xue, W., Li, X., Zhang, J., Chen, S., Zhang, J.L., Yang, L., and Chen, L.L. (2016a). The Biogenesis of Nascent Circular RNAs. *Cell Rep.* 15, 611–624.
- Zhang, Y., Yang, L., and Chen, L.L. (2016b). Characterization of Circular RNAs. *Methods Mol. Biol.* 1402, 215–227.
- Zheng, X., and Bevilacqua, P.C. (2004). Activation of the protein kinase PKR by short double-stranded RNAs with single-stranded tails. *RNA* 10, 1934–1945.

STAR★METHODS

KEY RESOURCES TABLE

| REAGENT or RESOURCE | SOURCE | IDENTIFIER |
|--|--------------------|-------------------------------|
| Antibodies | | |
| Anti-β-Actin | Sigma | Cat# A3854; RRID: AB_262011 |
| Anti-PKR | Abways | Cat# CY5665 |
| Anti-Phospho-PKR (T446) | Abways | Cat# CY5271 |
| Anti-rabbit-IgG-HRP | Santa Cruz | Cat# sc-2004; RRID: AB_631746 |
| Anti-mouse-IgG-HRP | Santa Cruz | Cat# sc-2005; RRID: AB_631736 |
| Anti-Flag | Sigma | Cat# F1804; RRID: AB_262044 |
| Mouse IgG | ABCBAM | Cat# ab18421 |
| Bacterial and virus strains | | |
| BL21 | Transgen Biotech | Cat# CD801 |
| T1 | Transgen Biotech | Cat# CD501-01 |
| Chemicals, peptides, and recombinant proteins | | |
| Poly(I:C) | Sigma | Cat# P9582 |
| 2-Aminopurine (2-AP) | Sigma | Cat# A3509 |
| Imidazolo-oxindole PKR inhibitor C16 | Sigma | Cat# I9785 |
| RNase R | Epicenter | Cat# MRNA092 |
| T4 RNA Ligase 1 | NEB | Cat# M0204L |
| Lipofectamine MessengerMAX reagent | Thermo | Cat# LMRNA008 |
| Ham's F-12K | GIBCO | Cat# 21127022 |
| FBS | Invitrogen | Cat# 10438-026 |
| Glutamax | Invitrogen | Cat# 35050061 |
| TRIzol Reagent | Ambion | Cat# 15596018 |
| DPBS | GIBCO | Cat# 14190-135 |
| Glycerol | ABCONE | Cat# G46055 |
| TWEEN 20 | ABCONE | Cat# P87875 |
| Agarose | ABCONE | Cat# A47902 |
| Bovine Serum Albumin | ABCONE | Cat# A23088 |
| 2-methylnicotinic acid imidazolide (NAI) | EMD Millipore | Cat# 03-310 |
| IFN γ | Sango Biotech | Cat# C600039 |
| Critical commercial assays | | |
| DIG Northern Starter Kit | Roche | Cat# 12039672910 |
| Hieff Clone One Step Cloning Kit | Yeasen | Cat# 10905ES25 |
| 2 × T5 Super PCR Mix | TSINGKE | Cat# TSE005 |
| SuperScript III Reverse Transcriptase | Invitrogen | Cat# 18080044 |
| SuperScript II Reverse Transcriptase | Invitrogen | Cat# 18064071 |
| Hifair III One step RT-qPCR Probe Kit | Yeasen | Cat# 11145 |
| RiboMAX Large Scale RNA Production System | Promega | Cat# P1300 |
| StarPrep Gel Extraction Kit StarPrep | GenStar | Cat# D205-04 |
| CellTiter 96 AQueous One Solution Cell Proliferation Assay | Promega | Cat# G3582 |
| 4.63 × 300 mm size exclusion column | Sepax Technologies | Cat# 215980P-4630 |
| Human IL-6 Valukine ELISA kit | R&D Systems | Cat# VAL 102 |
| Human IFN-beta Valukine ELISA kit | R&D Systems | Cat# VAL 137 |

(Continued on next page)

Continued

| REAGENT or RESOURCE | SOURCE | IDENTIFIER |
|--|--------------------------------------|---|
| Deposited data | | |
| <i>in vitro</i> circSHAPE-Map data | This paper | GEO: GSE183941 NODE: OEP002873 |
| Original unprocessed data were uploaded to Mendeley Data | This paper | https://doi.org/10.17632/yzsfgz7sp6.1 |
| Experimental models: Cell lines | | |
| A549 | ATCC | Cat# CCL-185 |
| HeLa | ATCC | Cat# CCL-2 |
| HEK293 | ATCC | Cat# CRL-1573 |
| 293FT | Thermo Fisher Scientific | Cat# R70007 |
| Recombinant DNA | | |
| pUC57- bacteriophage_td | (Wesselhoeft et al., 2018, 2019) | (Wesselhoeft et al., 2018, 2019) |
| pUC57-Anabaena_pre-tRNA | (Wesselhoeft et al., 2018, 2019) | N/A |
| pCRII- circPOLR2a_TD | This paper | N/A |
| pCRII- circPOLR2a_Ana | This paper | N/A |
| pCRII- circPOLR2a_Lig | This paper | N/A |
| pCRII- circCVB3-mCherry_TD | This paper | N/A |
| pUC57- circCVB3-mCherry_Ana | This paper | N/A |
| pUC57- circCVB3-mCherry_Lig | This paper | N/A |
| pCRII- circRTN4_TD | This paper | N/A |
| pCRII- RTN4_Ana | This paper | N/A |
| pCRII- circRTN4_Lig | This paper | N/A |
| pCRII- circCAMSAP1_TD | This paper | N/A |
| pCRII- circSMARCA5_Ana | This paper | N/A |
| pCDNA3- circPOLR2a_TD_Lig | This paper | N/A |
| pCDNA3- circPOLR2a_Ana_Lig | This paper | N/A |
| pET-28a-His-PKR | (Liu et al., 2019) | N/A |
| pET-28a-His-RIG-I | (Liu et al., 2019) | N/A |
| pLKO.1-TRC vector | (Moffat et al., 2006) | Addgene Plasmid # 10878 |
| p23-Flag-PACT | This paper | N/A |
| Software and algorithms | | |
| Cutadapt v2.10 | Cutadapt Software | https://cutadapt.readthedocs.io/en/v2.1/guide.html |
| Bowtie v2.1.0 | (Langmead and Salzberg, 2012) | http://bowtie-bio.sourceforge.net/bowtie2/index.shtml |
| CIRCshapemapper | (Guo et al., 2021; Liu et al., 2019) | https://github.com/YangLab/CIRCshapemapper |
| RNAfold v2.4.2 | (Lorenz et al., 2011) | https://www.tbi.univie.ac.at/RNA/ |
| StructureEditor v1.0 | RNA StructureEditor Software | http://rna.urmc.rochester.edu/GUI/html/StructureEditor.html |

RESOURCE AVAILABILITY

Lead contact

Further information and requests for resources and reagents should be directed to and will be fulfilled by the Lead Contact, Ling-Ling Chen (linglingchen@sibcb.ac.cn).

Materials availability

All unique/stable reagents generated in this study are available from the Lead Contact with a completed Materials Transfer Agreement.

Data and code availability

- All sequencing data reported in this paper have been deposited in the GEO (Gene Expression Omnibus, GSE183941) and NODE (National Omics Data Encyclopedia, OEP002873). All original unprocessed data related to this paper were uploaded to Mendeley Data (<https://doi.org/10.17632/yzsfgz7sp6.1>).
- This paper does not report original code.
- Any additional information required to reanalyze the data reported in this paper is available from the lead contact upon request.

EXPERIMENTAL MODEL AND SUBJECT DETAILS

Human cell lines

Human cell lines including A549, HeLa, HEK293 cells were purchased from the American Type Culture Collection (ATCC; <http://www.atcc.org>) and 293FT purchased from ThermoFisher.

Cell culture, transfection and stimulation

Human cell lines including A549, HeLa, HEK293 and 293FT cells were maintained using standard protocols from ATCC. RNAs synthesized *in vitro* and poly(I:C) were transfected using Lipofectamine MessengerMax reagent (Thermo) for A549, HeLa, HEK293 and 293FT cells according to the manufacturer's protocols. About 70%–80% transfection efficiency was achieved in cells. After transfection for 1 or 6 hours, protein or total RNAs were collected for analyses.

Bacterial strains

E.coli expression strain BL21 [Tranetta (DE3) chemically competent cell] were procured from Transgen Biotech (Cat# CD801) and were grown in LB culture at 37°C for protein purification.

METHOD DETAILS

Plasmid construction

To synthesize different circRNAs, group I self-splicing intron and IRES sequence were chemically synthesized (GenScript), and we constructed the T7 polymerase based expression vectors as *in vitro* transcription templates. All constructs were confirmed by Sanger sequencing. Sequences of spacer regions, group I self-splicing intron, and other minor alterations introduced were listed in [Table S2](#).

RNA isolation, RT-PCR, qRT-PCR and Northern Blotting (NB)

Total RNAs from cultured cells were extracted with Trizol (Life technologies) according to the manufacturer's protocol. RNAs were treated with DNase I (Ambion, DNA-free™ kit). cDNAs were reverse transcribed with SuperScript III (Invitrogen) and applied for PCR/qPCR analysis. 18S rRNA was examined as an internal control for normalization. Expression of each examined gene was determined from three independent experiments. Primers for qRT-PCR were listed in [Table S2](#).

NB was performed according to the manufacturer's protocol (DIG Northern Starter Kit, Roche). Digoxigenin (Dig)-labeled antisense riboprobes were made using RiboMAX Large Scale RNA Production Systems (Promega). In brief, 1 ng *in vitro* synthesized linear or circular RNAs was resolved on denaturing urea polyacrylamide gel, transferred to nylon membrane (Roche) and UV-crosslinked using standard manufacturer's protocol. Membrane was then hybridized with specific Dig-labeled riboRNA probes. NB probes were listed in [Table S2](#).

In vitro RNA transcription, circularization and purification

RNAs were *in vitro* transcribed from T7 expression vector prepared by RiboMax large RNA production system (Promega) according to the manufacturer's protocol with slight modifications. Briefly, circRNA precursors synthesized by method I (T4 RNA ligase 1) were transcribed from 1 µg PCR-amplified T7-DNA fragments, incubated with 2 µL T7 RNA polymerase enzyme in the presence of rATP, rCTP, rUTP, and GMP (each at 5 mM), rGTP (1 mM) for 3.5 hours at 37°C. Linear RNAs or circRNA precursors synthesized for self-splicing (T4 thymidylate synthase (*td*) gene and permuted Anabaena pre-tRNA, method II and method III, respectively) were synthesized in the same way by *in vitro* transcription in the presence of 5 mM rNTPs. *In vitro* transcription was followed by DNase I (Promega) treatment for 30 min at 37°C to remove DNA templates. Transcribed RNAs were column purified using a MEGAclear Transcription Clean-up kit (Invitrogen). For T4 RNA ligase 1 circularization system (Method I), 50 µg linear RNAs were incubated with T4 RNA ligase 1 (NEB) in 1mL reaction for 3 hours at 37°C according to the manufacturer's protocol. For group I intron autocatalytic splicing system (method II and method III), we used the group I intron of phage T4 thymidylate synthase (*td*) gene or permuted Anabaena pre-tRNA ([Wesselhoeft et al., 2018, 2019](#)), in which the *td* gene is different from the sequences from [Chen et al. \(2017\)](#) with a 34 nt extra spacer. 50 µg circRNA precursors were heated to 70°C for 3 min and immediately placed on ice for 2 min, then GTP was added to a final concentration of 2 mM with a buffer that has the same components as the T4 RNA ligase buffer (NEB) for 8 min at 55°C.

Circularized or linear RNAs were then concentrated by ethanol precipitation, resolved on denaturing urea polyacrylamide gel or agarose gel and visualized by Ethidium bromide staining. Of note, we routinely run circularized RNAs shorter than 1,500 nt on denaturing urea polyacrylamide gel; while circularized RNAs larger than 1,500 nt on native agarose gel with formamide and heat denaturing of the RNA before loading. Corresponding bands on denaturing urea polyacrylamide or native agarose gels were excised for circular or linear RNA purification (Figures S1 and S2). Purified circular or linear RNAs were validated by RNase R treatment normally for 45 min. Of note, different batches of RNase R were pre-determined for the use of concentrations (Zhang et al., 2016b). Primers for circularization were listed in Table S2.

High Performance Liquid Chromatography (HPLC)

HPLC fractionation was performed with a 4.6 × 300mm size exclusion column (Sepax Technologies, 215980P-4630) with particle size of 5 μm and pore size of 2000 Å, the same setting as previously reported (Chen et al., 2019; Wesselhoeft et al., 2019). Nuclease-free TE buffer (pH = 6.0) was used as the mobile phase at a flow rate of 0.35 mL/minute. RNA fractions were manually collected and then extracted prior to subjecting to the subsequent quality control and experimental analyses.

Protein expression and purification

Expression plasmids (with pET-28a as backbone vector) for His-tagged proteins (PKR and RIG-I) were individually transformed into *E.coli* expression strain BL21 [Transetta (DE3) chemically competent cell (Transgen Biotech, CD801)]. 5 mL LB culture supplemented with 100 μg/L kanamycin was incubated with a single colony at 250 rpm, 37°C. After overnight growth, the culture was diluted 100-fold into 100 mL LB culture supplemented with 100 μg/L kanamycin. Absorbance was monitored at a wavelength of 600 nm, and upon reaching an optical density (OD600) of 0.4, protein expression was induced by adding of 1 mM IPTG. After overnight incubation at 250 rpm, 16°C, cell pellets were harvested by centrifugation (5,000 rpm, 10 min, 4°C). Cell pellets were resuspended in lysis buffer (50 mM Tris pH 8.0, 300 mM NaCl, 20 mM imidazole, 1 mM PMSF) supplemented with 1 mg/mL lysozyme, and stored on ice for 30 min, followed by 10 min (5 s on/off) sonication on ice. After centrifugation at 10,000 rpm for 30 min at 4°C, the supernatant cell lysates were incubated with Ni Sepharose (GE healthcare) for 2 hours at 4°C. The Sepharose was washed 4 times with washing buffer (50 mM Tris pH 8.0, 300 mM NaCl, 40 mM imidazole, 1 mM PMSF), and bound protein was eluted with elution buffer (50 mM Tris pH 8.0, 300 mM NaCl, 300 mM imidazole). Elution was repeated twice to gain maximum yield. The concentration of purified protein was determined by using Modified Bradford Protein Assay Kit (Sangon Biotech, C503041) and checked by SDS-PAGE.

In vitro activation assay of PKR

In vitro activation assay of PKR was performed as described (Zheng and Bevilacqua, 2004) with modifications. Briefly, equal amounts of the purified top strand 79nt RNA (TS79R) and the bottom strand 79nt RNA (BS79R) were annealed in TEN₁₀₀ (10 mM Tris [pH 7.5], 1 mM EDTA, and 100 mM NaCl) for 1 min at 95°C followed by cooling on the bench for 10 min. Annealed duplexes were stored at -80°C and used at room temperature immediately after thawing. The ability of various RNAs to activate or inhibit PKR kinase was determined by PKR auto-phosphorylation assays. Purified PKR was first dephosphorylated by treating with λ-PPase (NEB), as described (Matsui et al., 2001). Subsequently, λ-PPase was inactivated by treatment with freshly prepared sodium orthovanadate (Matsui et al., 2001). Next, 10 μCi [γ -³²P] ATP, 0.6 μM dephosphorylated PKR, and different RNAs were incubated in 20 mM HEPES (pH 7.5), 4 mM MgCl₂, 100 mM KCl, and 1 mM ATP for 30 min at 30°C. Reactions were stopped by adding SDS loading buffer and analyzed on a 10% SDS-polyacrylamide gel. PKR amounts among samples were verified by Western Blotting with antibodies (Abways) against PKR.

Enzyme-linked immunosorbent assay (ELISA)

Cell culture supernatant was collected by removing pellets by centrifugation at 1000 rpm. The resulting samples were immediately stored at -20°C. ELISA kits for human IFNβ and IL-6 were purchased from R&D Systems. Cytokines were detected by solid phase sandwich ELISA (R&D Systems) according to the manufacturer's instructions.

Cell proliferation assay

1 × 10³ A549 cells transfected with indicated RNAs (Figure S9A) were seeded in 96-well and cell numbers were measured every 24h according to CellTiter 96 AQueous One Solution Cell Proliferation Assay (Promega). Data were presented with respect to 0 h cells set to a value of 1.

In vitro SHAPE probing (with/without proteins)

In vitro SHAPE probing was performed as described (Guo et al., 2021; Liu et al., 2019; Smola et al., 2015) with modifications. In brief, *in vitro* produced and purified human 5S rRNA/circular RNAs were refolded in 3.3 × folding buffer (333 mM HEPES, pH 8.0; 333 mM NaCl; 33 mM MgCl₂). After refolding, RNAs were incubated with 10x SHAPE Chemical in DMSO with the final concentration of NAI (EMD Millipore) at 100 mM for 10 minutes at 37°C. For *in vitro* SHAPE probing with proteins, purified PKR/RIG-I were incubated with refolded RNAs respectively, following by modification with NAI at 100 mM or with DMSO for 10 minutes at 37°C. Two control reactions were performed in parallel: a no-reagent control and a denaturing control. In the no-reagent control reaction, folded

RNA is incubated with solvent only (typically DMSO for NAI reagents); this control measures the intrinsic background mutation rate of reverse transcriptase under MaP conditions and also detects certain naturally occurring RNA modification events. In the denaturing control reaction, RNAs were suspended in a denaturing buffer containing formamide and incubated at 95°C prior to modification with NAI. Nucleotides are modified relatively evenly in this step, and the resulting site-specific mutation rates account for subtle sequence- and structure-specific biases in detection of adduct-induced mutations. Thus, a complete *in vitro* SHAPE-MaP experiment consists of three reactions: plus-reagent (+), minus-reagent (-), and denaturing control (DC).

SHAPE-MaP reverse transcription

Isolated RNAs were treated with DNase I (Ambion, DNA-free™ kit) to remove possible DNA contamination. About 50-100 ng of RNAs were obtained under each treatment, and were then used for SHAPE-MaP reverse transcription by adding 1 µL (200 U/µL) of SuperScript II (Invitrogen), 6 mM Mn²⁺ and gene-specific primers for linear or circular RNAs (5S rRNA was used as a spike-in control). All primers were listed in [Table S2](#). Mn²⁺ was removed using G-25 micro-spin columns (GE Healthcare) after SHAPE-MaP reverse transcription. Second-strand synthesis was performed with Q5 hot start high-fidelity DNA polymerase and nested PCR was performed to further improve DNA yield. The resulting PCR products were further isolated with PureLink micr spin columns (Life Technologies). Primers for SHAPE-MaP reverse transcription and second-strand synthesis (1st round PCR and nested PCR reactions) were listed in [Table S2](#). Of note, 6 nt barcodes were added in 5' end of revers primer to identify different circularization strategies.

SHAPE-MaP library preparation and sequencing

In vitro synthesized circular RNAs at each condition as one sample was used to build library. In brief, SHAPE-MaP libraries were prepared from 1 ng of DNAs reverse-transcribed from circular SHAPE RNA, and size-selected with AmpureXP beads (Agencourt) with a 1:1 (bead to sample) ratio to obtain library DNA products spanning 100-400 bp in length. Final libraries were quantified using Agilent Bioanalyzer 2100 and QuBit high-sensitivity dsDNA assay. Deep sequencing was performed by Illumina HiSeq X Ten platform at CAS Key Laboratory of Computational Biology Omics Core, Shanghai, China. About 5-15 million sequencing reads were obtained for each sample, with 86% of bases at or above Q30.

Co-Immunoprecipitation (IP)

A549 cells expressing flag-PACT (2×10^7) were transfected with 1 µg *circPOLR2A_Lig*, and IFNγ was added at 12 hours post-transfection. Then, cells were harvested and suspended in 1 mL lysis buffer [50 mM Tris pH 7.4, 150 mM NaCl, 0.05% Igepal, 0.5% NP-40, 0.5 mM PMSF, 2 mM RVC, protease inhibitor cocktail (Roche)] followed by 3 × 10 s sonication. After incubation with 2 µg anti-flag antibody (Sigma) or anti-mouse IgG antibody (Sigma), the beads were washed 4 × 5 min with wash buffer [50 mM Tris pH 7.4, 300 mM NaCl, 0.05% Sodium Deoxycholate, 0.5% NP-40, 0.5 mM PMSF, 2 mM RVC, protease inhibitor cocktail (Roche)]. To harvest the protein complex, 50 µL of 1 × SDS loading buffer (62.4 mM Tris pH 6.8, 10% glycerol, 2% SDS, 0.0012% bromophenol blue) was added, boiled for 10 min at 100°C, and analyzed by WB.

QUANTIFICATION AND STATISTICAL ANALYSIS

CircSHAPE-MaP data analyses

CircSHAPE-MaP libraries of circular RNAs were prepared by mixed production from circular RNAs reverse transcription. To separate circSHAPE-MaP data of each circular RNA, the reverse PCR primer were added 6 nt barcode at the 5' end ([Table S2](#)) and recognized by Cutadapt (v2.10, <https://cutadapt.readthedocs.io/en/v2.1/guide.html>). Of note, the barcode was located either on R1 and R2 because of the library were built by cDNA. Data were separated according barcodes in R1 first with parameter: -g file:barcode.fa -G file:barcode.fa -pair-filter = both -O 23 -e 0.0 -match-read-wildcards-action = none -o Round1_{name}_R1.fastq -p Round1_{name}_R2.fastq circSHAPE-MaP_R1.fastq circSHAPE-MaP_R2.fastq. All the reads with no barcode in R1 were end up in Round1_unknown_R1.fastq and Round1_unknown_R2.fastq. Then the “unknown” data were separated by running Cutadapt second time with paratemer: -g file:barcode.fa -G file:barcode.fa -pair-filter = both -O 23 -e 0.0 -match-read-wildcards-action = none -o Round2_{name}_R2.fastq -p Round2_{name}_R1.fastq Round1_unknown_R2.fastq Round1_unknown_R1.fastq.

After data separation, the circSHAPE-MaP data of each circular RNA was analyzed by CIRCshapemapper pipeline which was built up in our previous study (Liu et al., 2019; Smola et al., 2015). In brief, the target circular RNA sequence and three circSHAPE-MaP datasets (NAI modified data, denatured control (DC) data and DMSO data) were input into the pipeline including data pre-treatment, two-round alignment, mutation calling and SHAPE reactivity calculation. The pre-treatment step was used to control quality of the input data and build index. Two-round alignment was designed to improve mapping accuracy. Then the mapped reads were parsed to count mutation rate of each site and the SHAPE reactivity was calculated by [(Modified_{MutR}-Untreated_{MutR})/Denatured_{MutR}]. Next, SHAPE reactivity was used for structure modeling with circRNA sequence.

circRNA secondary structure modeling

The circular RNA secondary structure was modeled by RNAfold(v2.4.2) (parameter: -p -d2 -shape = SHAPE profile -shapeMethod = D -circ < circRNA.fa) with SHAPE reactivity generated by CIRCshapemapper. And the structure was visualized by StructureEditor

with SHAPE reactivity. In addition, the structure of extra E1, E2 and spacer fragments from T4 phage *td* intron or Anabaena intron genes were modeled by RNAfold (parameter: -p -d2 < RNA.fa) without SHAPE reactivity ([Figures S4B](#) and [S4C](#)).

Statistical analysis

Statistical significance for comparisons of means was generally assessed by Student's t test with exceptions described below. $p < 0.05$ was marked by 1 asterisk, while 2 asterisks indicated $p < 0.01$ and 3 asterisks $p < 0.001$.

Supplemental information

**RNA circles with minimized immunogenicity
as potent PKR inhibitors**

Chu-Xiao Liu, Si-Kun Guo, Fang Nan, Yi-Feng Xu, Li Yang, and Ling-Ling Chen

Supplemental Figures and Figure legends

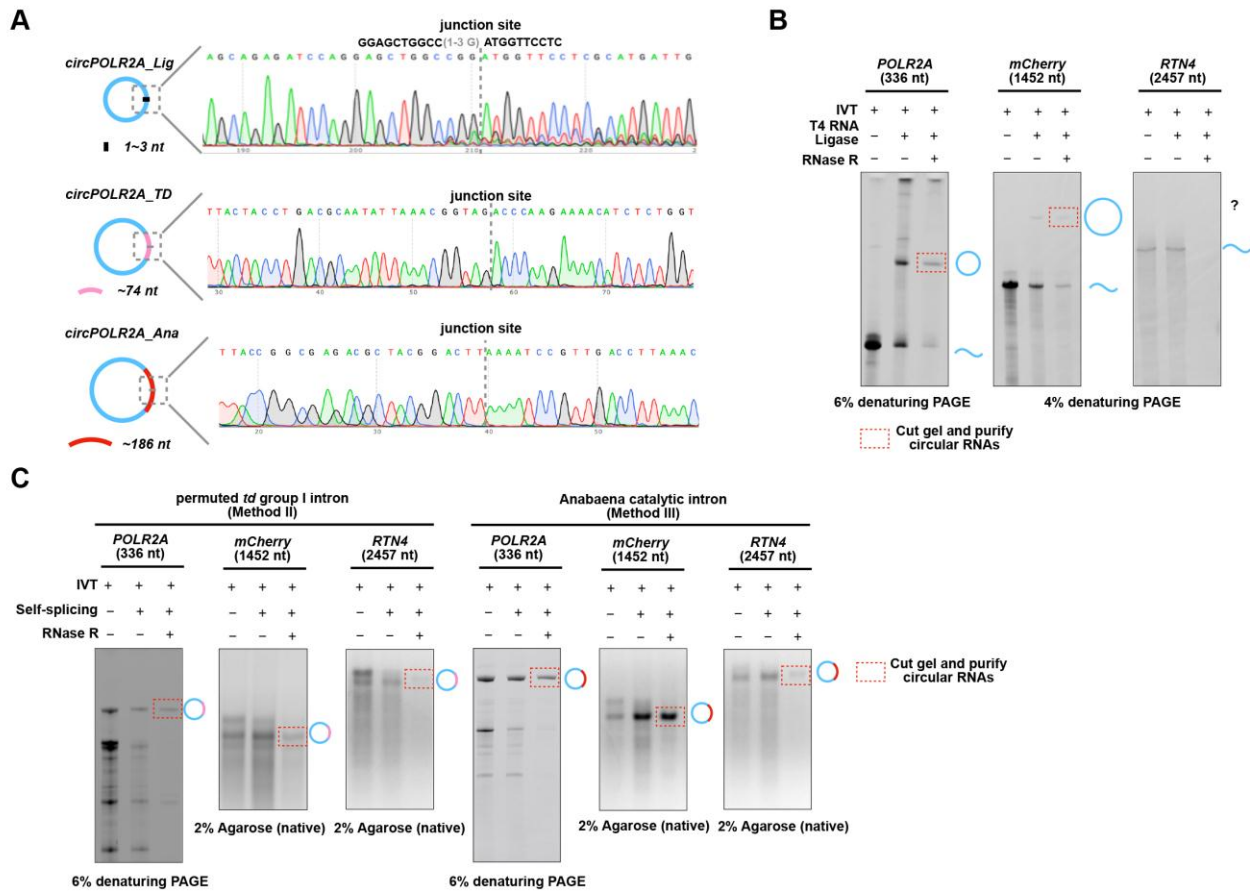


Figure S1. Overview of different strategies for production of circular RNAs *in vitro*. (Related to Figure 1)

(A) Confirmation of junction sites of *circPOLR2A* produced by methods shown in Figure 1A by Sanger sequencing. Top: *CircPOLR2A_Lig* introduced 1~3 extra Guanine (G) nucleotides after circularization at the junction site. Middle and bottom: *circPOLR2A_TD* and *circPOLR2A_Ana* introduced 74 or 186 extraneous nucleotides into RNA circles, respectively, after autocatalytic circularization at their respective junction sites.

(B) Examination of circularization efficiency of three circular RNAs (*circPOLR2A*, 336 nt, *circmCherry*, 1,452 nt and *circRTN4*, 2,457 nt) using the exact same procedure by Method I. Of note, Method I could efficiently produce *circPOLR2A*, but produce *circmCherry* to a lower level and barely produce *circRTN4*.

(C) Examination of circularization efficiency of three circular RNAs (*circPOLR2A*, *circmCherry*, and *circRTN4*) using Methods II and III. Methods II and III produced *circPOLR2A* with comparable efficiency as Method I, but they generated *circmCherry* and *circRTN4* with a higher efficiency.

In (B) (C), *in vitro* circularized RNAs used in the current study were purified by cutting the circular RNA bands (indicated by red dotted boxes) on denaturing PAGE followed by purification steps.

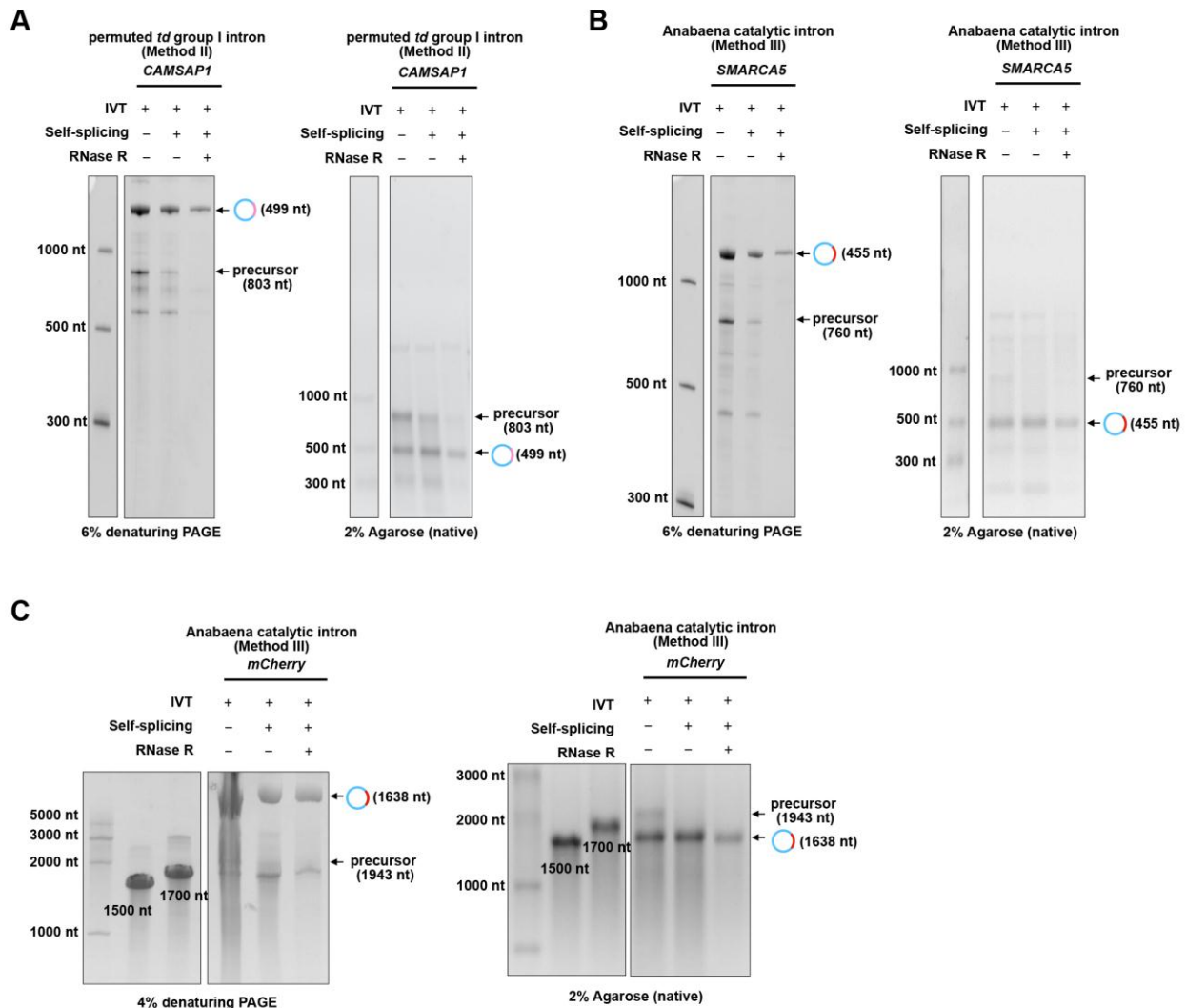


Figure S2. *In vitro* circularized RNAs and their precursor RNAs on denaturing PAGE and native agarose gels. (Related to Figure 1)

(A) Migration of *circCAMSAP1_TD* synthesized by Method II on PAGE (left) and agarose (right) gels. *CircCAMSAP1_TD* (499 nt) migrates more slowly than its linear precursor RNA (803 nt) on denaturing gels (6% PAGE), but migrates faster on native gels (2% agarose) in accordance to its molecular size.

(B) Migration of *circSMARCA5_Ana* synthesized by Method III on PAGE (left) and agarose (right) gels. *CircSMARCA5_Ana* (455 nt) migrates more slowly than its linear precursor RNA (760 nt) on denaturing gels (6% PAGE), but migrates faster on native gels (2% agarose) in accordance to its molecular size.

(C) Migration of long circular RNAs, using *circmCherry-Ana* (1,638 nt) synthesized by Method III as an example, on PAGE (left) and agarose (right) gels. *circmCherry-Ana* migrates more slowly than its linear precursor RNA (1,943 nt) on denaturing gels (4% PAGE), but migrates faster on native gels (2% agarose) in accordance to its molecular size. Of note, 1,500 nt and 1,700 nt single stranded (ss) RNAs were produced as controls in addition to the ssRNA ladder.

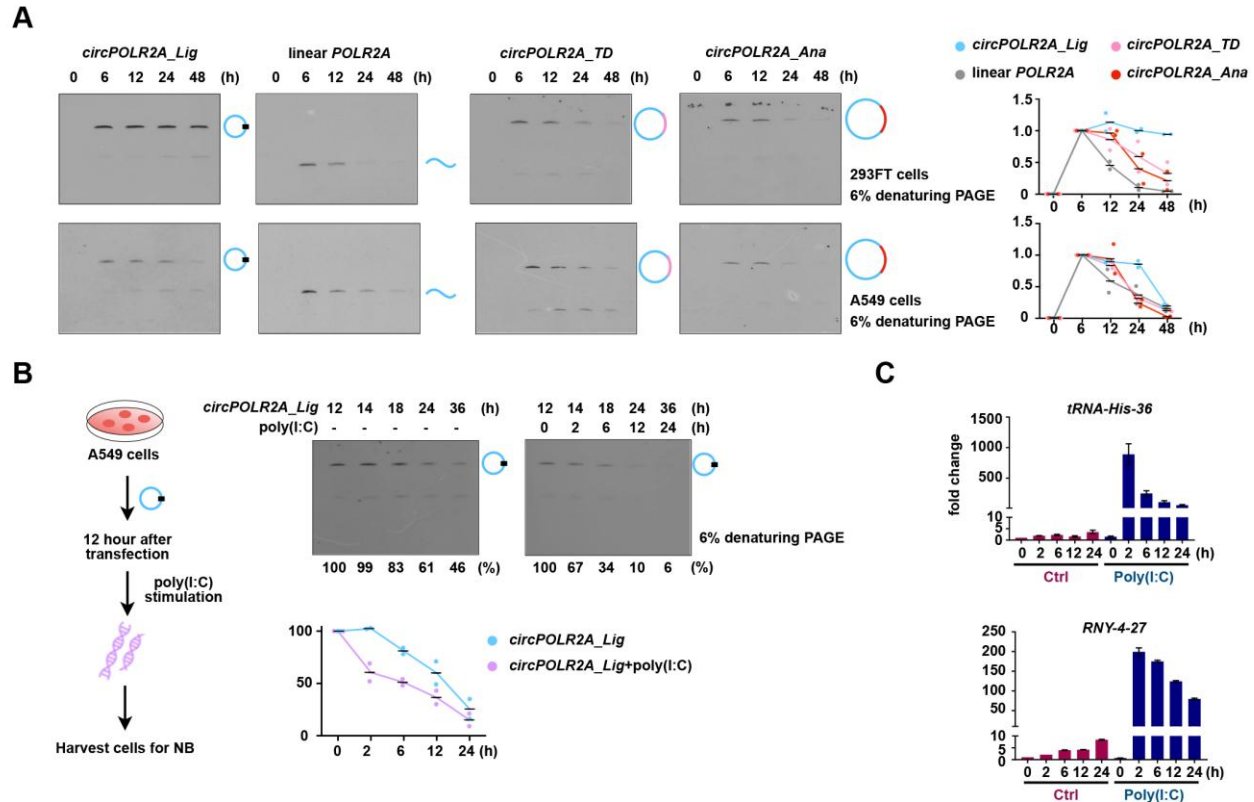


Figure S3. *In vitro* synthesized RNA circles are more stable than linear cognate RNAs and are also subjected to rapid turnover upon poly(I:C) stimulation. (Related to Figure 1)

(A) Stability of RNA circles (*circPOLR2A_Lig*, *circPOLR2A_TD* and *circPOLR2A_Anna*) as well as linear *POLR2A* in examined cells (293FT and A549 cells). The same amounts of RNA circles and linear *POLR2A* (200 ng for each sample) were transfected into 293FT and A549 cells, respectively. Total RNAs were collected at indicated time points and analyzed by denaturing NB.

(B) *In vitro* synthesized *circPOLR2A_Lig* undergoes rapid degradation under poly(I:C) stimulation. Examination of the stability of *circPOLR2A_Lig* in A549 cells under poly(I:C) stimulation by denaturing NB at indicated time courses 12 hours post transfection.

(C) Examination of RNase L cleavage activity. Relative expression of RNA products (*tRNA-His-36* and *RNY4-27*) after the activated RNase L were examined by qRT-PCR at indicated time courses. Error bars represent SD.

In (A) and (B), quantification of results shown in each cell line was performed from duplicated assays. Images were quantified by Quantity One and each dot represents the result from one assay at the indicated time.

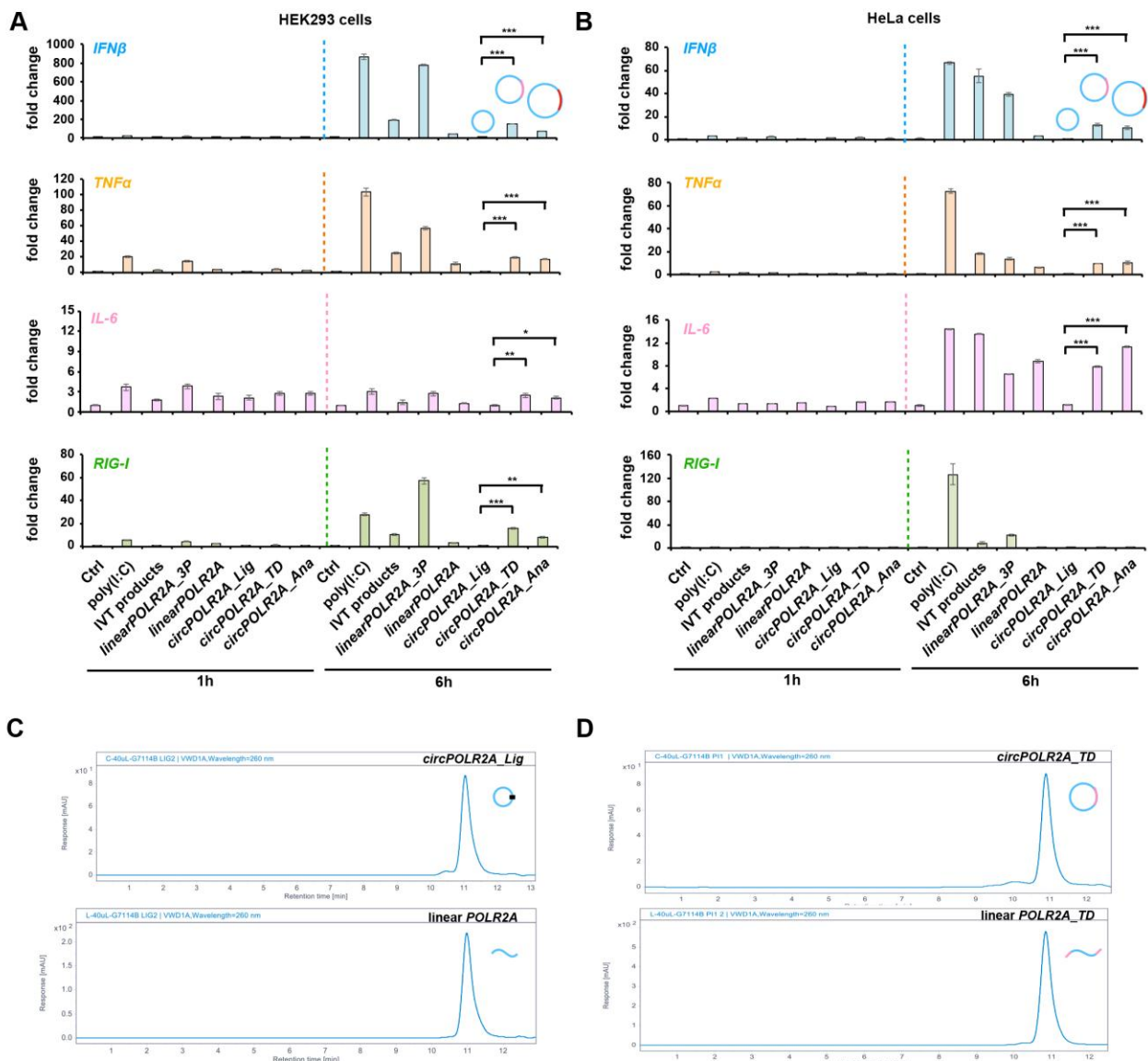


Figure S4. Circular RNAs produced from different *in vitro* circularization strategies induce distinct immune responses in human cells. (Related to Figure 1)

(A) Short circular RNAs, *circPOLR2A*, produced via group I intron splicing (Methods II and III) stimulate immune responses, while those produced from direct ligation (Method I) does not, in HEK293 cells.

(B) Short circular RNAs, *circPOLR2A*, produced via group I intron splicing (Methods II and III) stimulate immune responses, while those produced from direct ligation (Method I) does not, in HeLa cells.

(C-D) Size exclusion chromatography appears incapable of resolving *circPOLR2A_Lig* or *circPOLR2A_TD*. *circPOLR2A_Lig* or *circPOLR2A_TD* was first purified by RNase R digestion, gel excision and purification, followed by subjected to HPLC analyses. The corresponding linear RNA was also gel purified prior to HPLC analysis. Of note, the peaks of gel purified circular and linear *circPOLR2A_Lig* or *circPOLR2A_TD* products in HPLC were totally overlapped.

In (A) (B), the same amounts (200 ng for each sample) of different RNAs were individually transfected into HEK293 (A) or HeLa (B) cells, see Figure 1C for details. Error bars represent SD.
*p<0.05, **p<0.01, ***p<0.001, Student's t test.

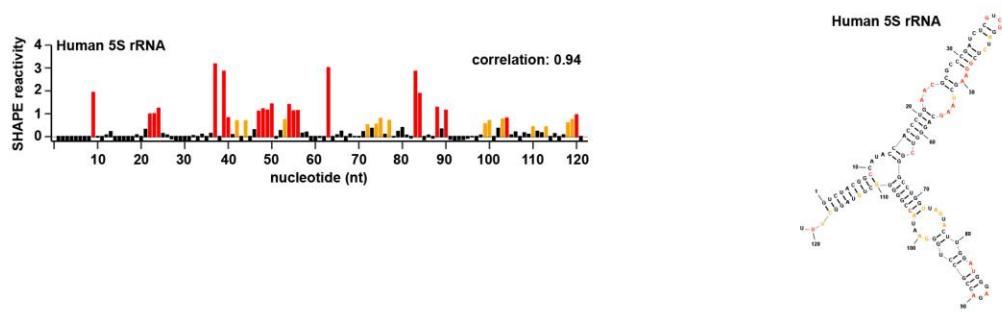
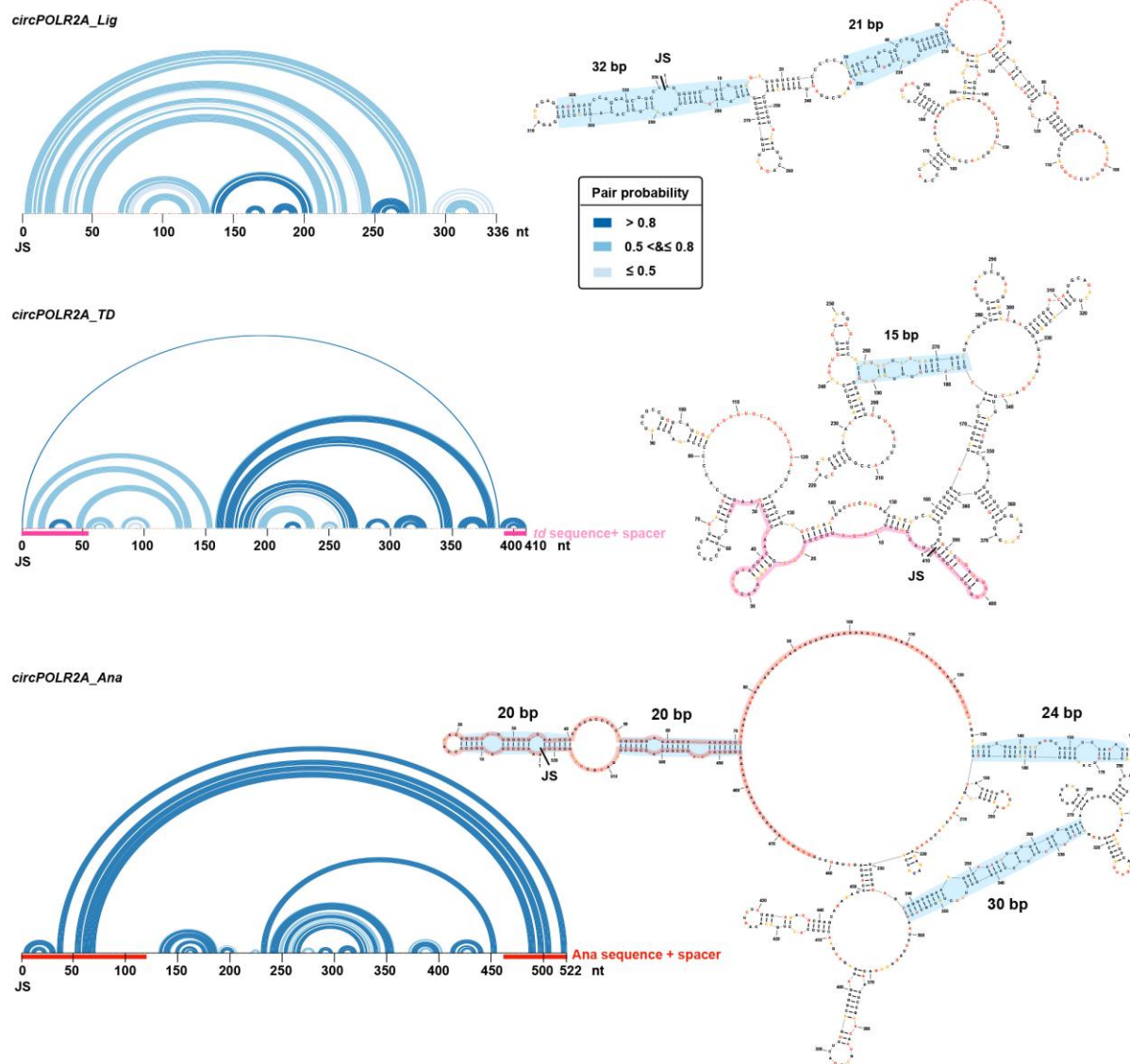
A**B**

Figure S5. Structural conformation of examined circRNAs *in vitro*. (Related to Figure 3)

(A) Secondary structural model of human 5S rRNA revealed by *in vitro* SHAPE-MaP. Left: red, orange and black colors are corresponding to high, moderate and low reactivities, respectively. Spearman's rank correlation coefficient of human 5S rRNA is high in SHAPE-MaP (0.94),

suggesting the high reproducibility of SHAPE assays. Right: the secondary structural model of human 5S rRNA revealed by *in vitro* SHAPE-MaP predicted with SHAPE values.

(B) The secondary structural models of *circPOLR2A_Lig*, *circPOLR2A_TD* and *circPOLR2A_AnA* revealed by *in vitro* SHAPE-MaP predicted by RNAfold with SHAPE values. Potential base pairs are shown as color arcs indicating pair probabilities. Pink and red lines indicate the extra fragments introduced by autocatalytic splicing. Potential intra-dsRNA regions (length >16 bp but <33 bp) formed in *circPOLR2A_Lig*, *circPOLR2A_TD* and *circPOLR2A_AnA* are illustrated (blue shadows).

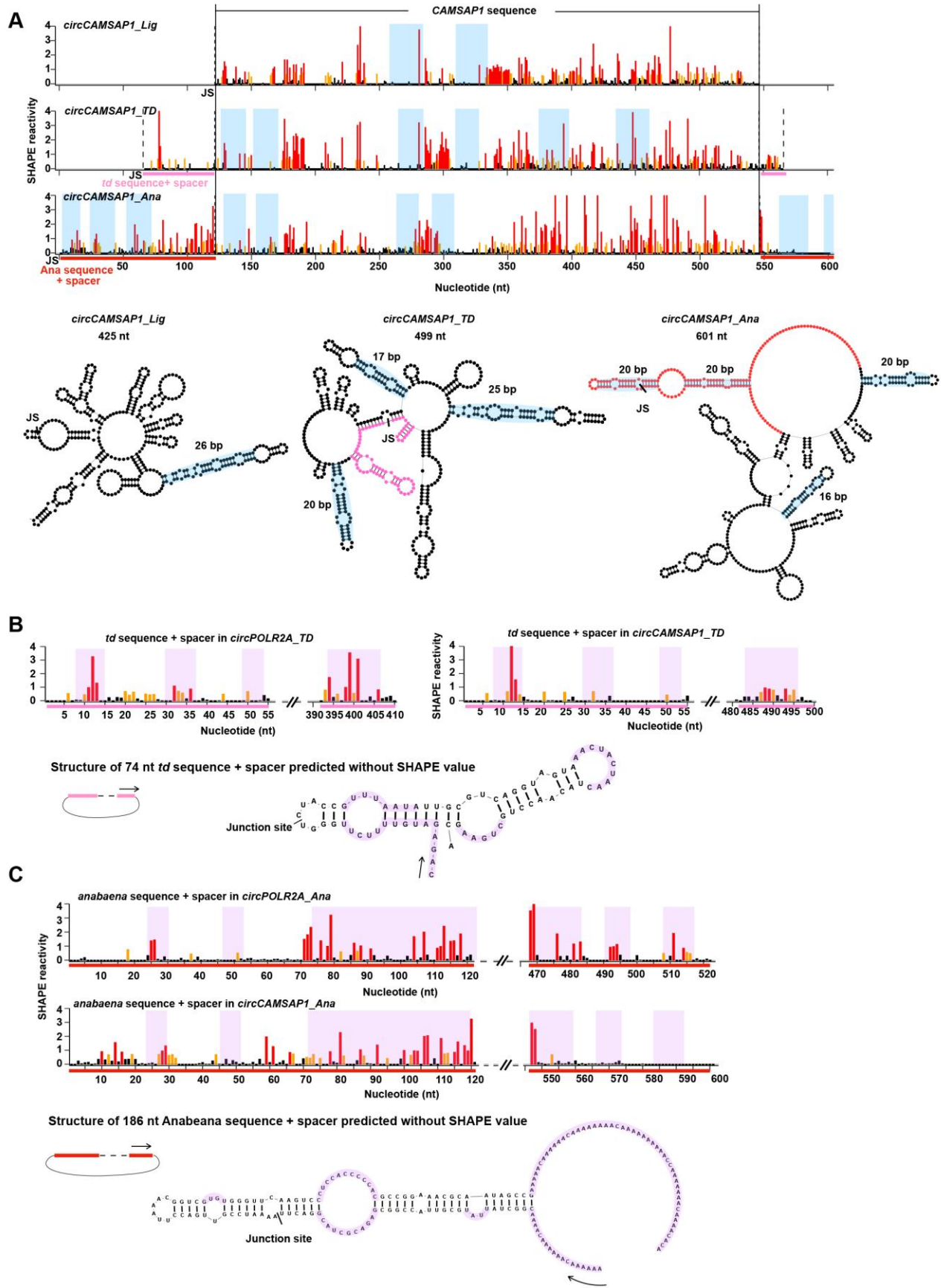


Figure S6. Autocatalytic splicing introduces ~74 nt *td* and ~186 nt pre-tRNA extraneous fragments in circular RNAs that tend to form long dsRNA duplexes. (Related to Figure 3)

(A) Top: circSHAPE-Map profiles of *circCAMSAP1_Lig*, *circCAMSAP1_TD* and *circCAMSAP1_Ana*. Pink and red line indicate the extra fragments introduced by autocatalytic splicing. Bottom: the predicted secondary structural models of *circCAMSAP1_Lig*, *circCAMSAP1_TD* and *circCAMSAP1_Ana* from *in vitro* circSHAPE-MaP. The imperfect short RNA duplexes of 16-33 bp in length are indicated in blue shadows.

(B) The predicted secondary structural model of the 74 nt *td* extraneous fragments in *circPOLR2A_TD* and *circCAMSAP1_TD*, which tend to form an imperfect dsRNA region longer than 35 bp. Top: circSHAPE-Map profiles of *circPOLR2A_TD* and *circCAMSAP1_TD*. Bottom: The secondary structural model of the 74 nt exogenous sequence without SHAPE values predicted *in silico*. Pink lines denote RNA regions that have similar SHAPE reactivities in *circPOLR2A_TD* and *circCAMSAP1_TD*. SHAPE reactivities that denote the corresponding predicted secondary structural models are shown.

(C) The predicted secondary structural model of the 186 nt extraneous sequences in *circPOLR2A_Ana* and *circCAMSAP1_Ana*, which tend to form an imperfect dsRNA region longer than 50 bp. Top: circSHAPE-Map profiles of *circPOLR2A_Ana* and *circCAMSAP1_Ana*. Bottom: the secondary structural model of the 186 nt exogenous sequence without SHAPE values predicted *in silico*. Pink lines denote RNA regions that have similar SHAPE reactivities in *circPOLR2A_Ana* and *circCAMSAP1_Ana*. SHAPE reactivities that denote corresponding predicted secondary structural models are shown.

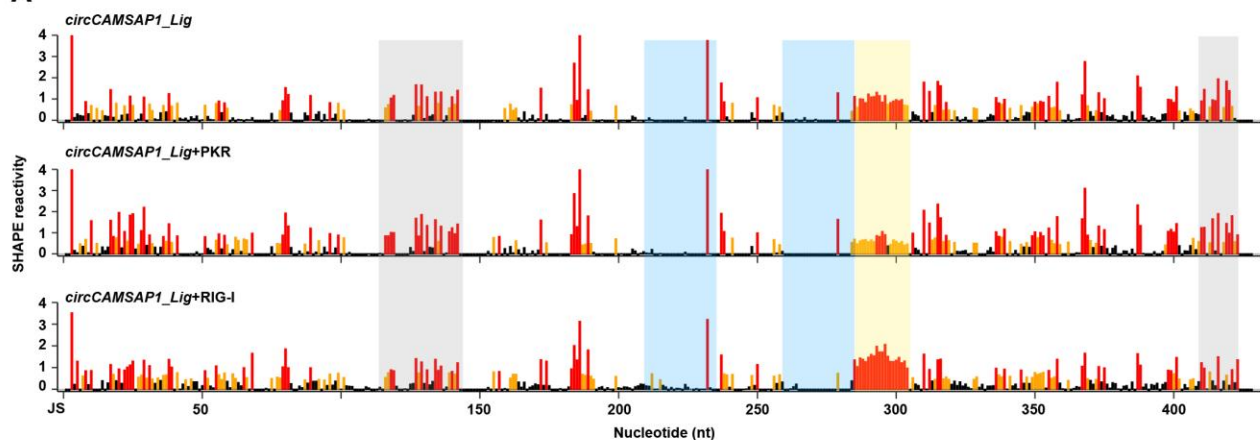
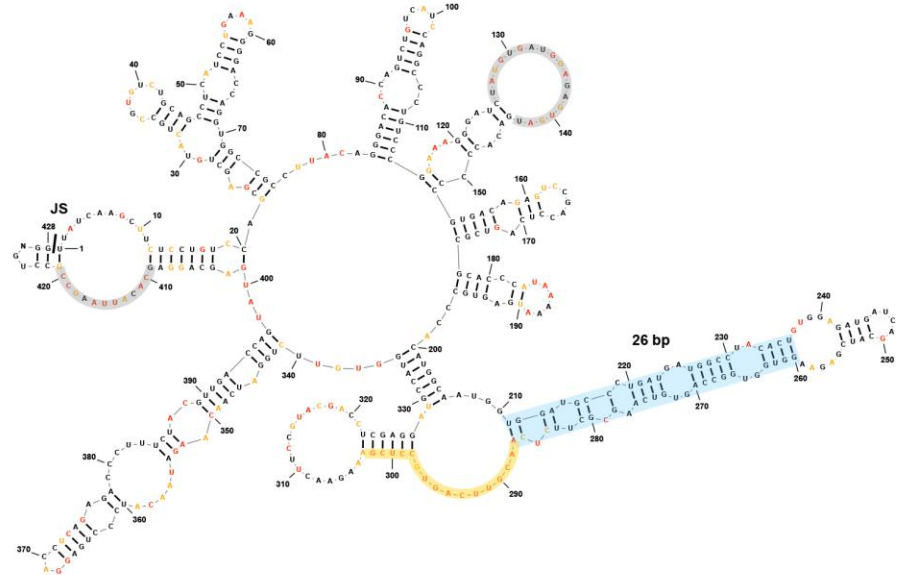
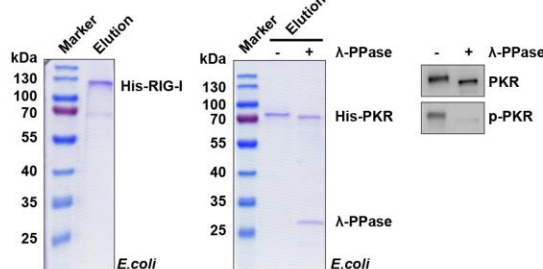
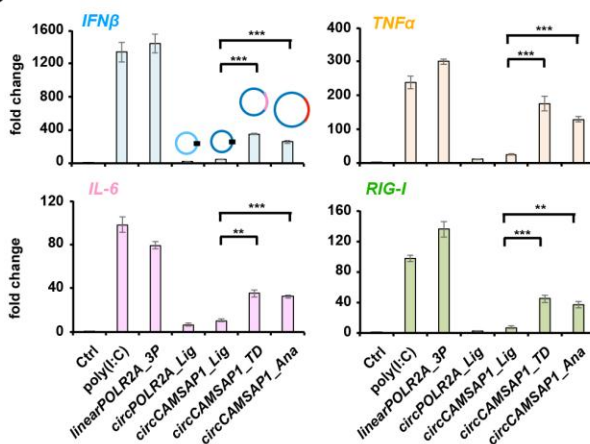
A**B****C****D**

Figure S7. The secondary structural models of *circCAMSAP1_TD* and *circCAMSAP1_AnA*, supplemented with dephosphorylated PKR or RIG-I. (Related to Figure 3)

(A) *In vitro* circSHAPE-Map reactivities of *circCAMSAP1_Lig* (upper), supplemented with purified and dephosphorylated PKR proteins (middle), or RIG-I proteins (bottom). The yellow shadow

denotes the reduced SHAPE reactivities upon PKR addition; the two grey shadows denote the unaltered high SHAPE reactivities upon PKR addition.

(B) The predicted secondary structural model of *circCAMSAP1_Lig*, which contains an imperfect dsRNA module (blue shadows, 26 bp). The yellow line denotes the reduced SHAPE reactivities showing the altered ssRNA region close to the imperfect dsRNA region upon PKR addition. The two grey lines denote the unaltered SHAPE reactivities showing the two unaltered ssRNA regions upon PKR addition, as controls.

(C) Purified PKR, dephosphorylated PKR and RIG-I proteins. Left, proteins purified from *E. coli* were shown by SDS-PAGE and Coomassie Blue staining. Right, phosphorylation of PKR and dephosphorylated PKR upon λ-PPase treatment were verified by WB.

(D) *CircCAMSAP1*, produced via group I intron splicing (Methods II and III) stimulates immune responses, while those produced from the direct ligation (Method I) does not. The same amounts (200 ng for each sample) of different RNAs were individually transfected into A549 cells, see Figure 1C for details. Error bars represent SD. **p<0.01, ***p<0.001, Student's t test.

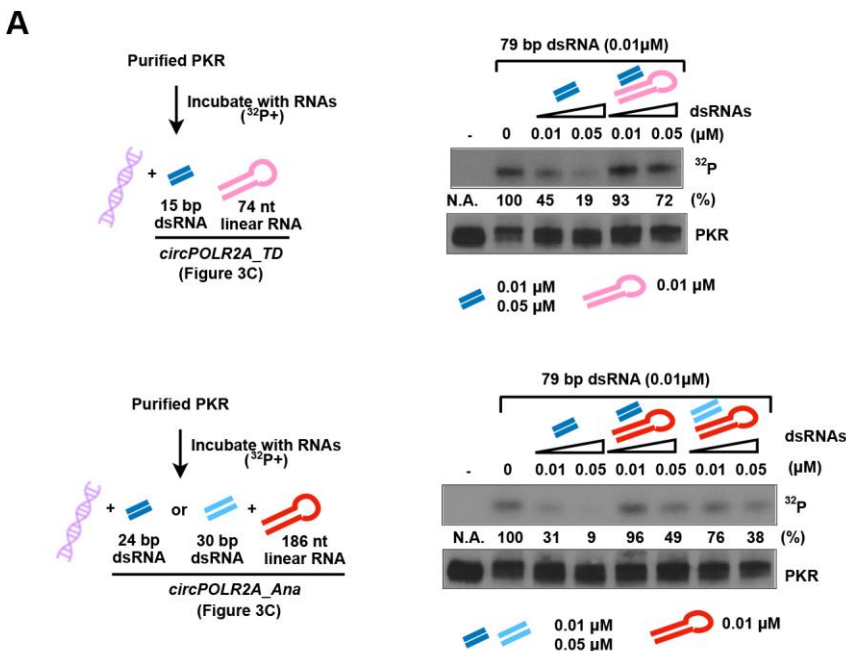


Figure S8. The 74 nt and 186 nt extraneous fragments dominate the short dsRNAs in the same RNA circles to stimulate PKR activation. (Related to Figure 4)

(A) Competitive *in vitro* PKR activation assays showed that 74 nt (top) and 186 nt (bottom) extraneous fragments dampened the inhibitory effect on PKR activation by the imperfect short RNA duplexes from the same RNA circles, respectively. *In vitro* PKR activation assays were

performed as shown in Figure 4A. Experiments were independently repeated and similar results were observed. The level of p-PKR in each panel was quantified by Quantity One, and p-PKR levels were normalized by PKR, respectively.

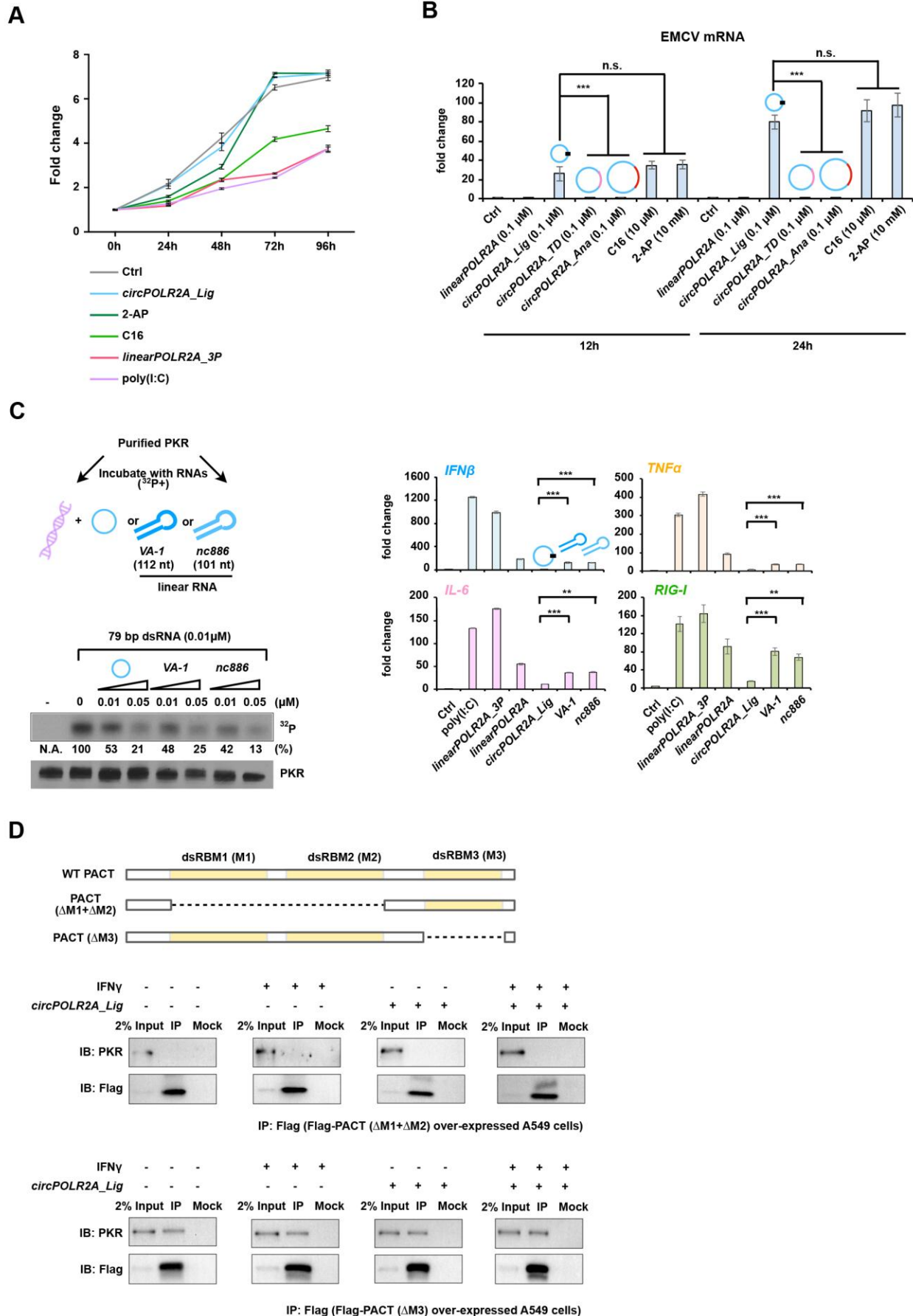


Figure S9. *CircPOLR2A_Lig* facilitated EMCV replication and inhibited PKR activation comparable to VA-1 or nc886. (Related to Figures 5 and 6)

(A) C16 suppressed A549 cells proliferation, but *circPOLR2A_Lig* transfection had little effect on cell proliferation, as shown by cell proliferation assays (CellTiter 96 AQueous One Solution Cell Proliferation Assay, Promega). Error bars represent SD in triplicate experiments.

(B) *CircPOLR2A_Lig* (0.1 μ M) facilitated EMCV replication at a comparable level to C16 (10 μ M) and 2-AP (10 mM) in A549 cells. Different RNAs and small molecules were transfected for 6 hours in A549 cells, followed by EMCV infection for 12 or 24 hours. Total RNAs were collected under each condition to examine EMCV mRNAs by qRT-PCR.

(C) VA-1 and nc886 both suppressed PKR activation, but are immunogenic. Left, VA-1 and nc886 showed a comparable level of inhibitory effect on PKR activation as *circPOLR2A_Lig* did. Left, these examined RNAs suppresses the *in vitro* activation of PKR (0.6 μ M) induced by 79 bp dsRNA (0.01 μ M) with an autoradiography using γ -³²P-ATP. Experiments were independently repeated and similar results were observed. The level of p-PKR in each panel was quantified by Quantity One, and p-PKR levels were normalized by PKR, respectively.

Right, transfection of VA-1 and nc886 into A549 cells individually both induced expression of inflammatory factors as shown by qRT-PCR; whereas transfection of *circPOLR2A_Lig* barely induced immune responses.

(D) *circPOLR2A_Lig* has no effect on PKR binding to PACT mutants ($\Delta M1+\Delta M2$ or $\Delta M3$) before and after IFN γ stimulation. Top, a schematic of PACT and PACT truncations lacking dsRBM1 +dsRBM2 ($\Delta M1+\Delta M2$) or dsRBM3 ($\Delta M3$). Bottom, Flag-PACT truncation-overexpressed A549 cell lines were generated ,followed by using co-immunoprecipitation to detect interactions between PKR and PACT truncations. *CircPOLR2A_Lig* did not affect PKR binding to PACT truncations before or after IFN γ stimulations. Experiments were independently repeated and similar results were observed.

(B)(C) Error bars represent SD. n.s., p > 0.05, **p<0.01, ***p<0.001, Student's t test.

Supplemental tables

Table S1. Spearman correlation of duplicate assays of circSHAPE-MaP. (Related to Figures 3, S5-S7)

| Spearman correlation of two repeats of circSHAPE-MaP | | | |
|--|---------------|-------------|---------------|
| Method I | circRNA | circRNA+PKR | circRNA+RIG-I |
| <i>circCAMSAPI</i> | 0.92276 | 0.970489 | 0.977004 |
| <i>circPOLR2A</i> | 0.993743 | 0.96432 | 0.98937 |
| Method II | circRNA | circRNA+PKR | circRNA+RIG-I |
| <i>circCAMSAPI</i> | 0.959056 | 0.953867 | 0.964178 |
| <i>circPOLR2A</i> | 0.979266 | 0.976359 | 0.983862 |
| Method III | circRNA | circRNA+PKR | circRNA+RIG-I |
| <i>circCAMSAPI</i> | 0.848192 | 0.818676 | 0.839211 |
| <i>circPOLR2A</i> | 0.954118 | 0.946966 | 0.89923 |
| internal control | human 5S rRNA | | |
| | 0.94 | | |